From Pyridine Adduct of Borabenzene to (in)finite Graphene Architectures Functionalized with N→B Dative Bonds. Prototype Systems of Strong One and Two Photon Quantum Transitions Triggering Large Nonlinear Optical Responses

Panaghiotis Karamanis, Nicolás Otero, Demetrios Xenides, Hassan Denawi, Marcos Mandado, Michel Rérat

From Pyridine Adduct of Borabenzene to (in)finite Graphene Architectures Functionalized with N→B Dative Bonds. Prototype Systems of Strong One and Two Photon Quantum Transitions Triggering Large Nonlinear Optical Responses

Journal:	*The Journal of Physical Chemistry*
Manuscript ID	jp-2020-05190a.R2
Manuscript Type:	Article
Date Submitted by the Author:	n/a
Complete List of Authors:	Karamanis, Panaghiotis; Institut des Sciences Analytiques et de Physico-chimie pour l'Environnement et les Materiaux, Otero, Nicolás; University of Vigo - Lagoas Marcosende Campus Xenides, Demetrios; University of Patras Denawi, Hassan; Aix-Marseille Universite, IPREM Mandado, Marcos; Universidade de Vigo, Physical Chemistry Rérat, Michel; IPREM / UPPA, STEE

From Pyridine Adduct of Borabenzene to (in)finite Graphene Architectures Functionalized with N→B Dative Bonds. Prototype systems of Strong One and Two Photon Quantum Transitions Triggering Large Nonlinear Optical Responses.

Panaghiotis Karamanis,*[a] Nicolás Otero,[b] Demetrios Xenides,[c] Hassan Denawi,[a] Marcos Mandado[b] and Michel Rérat[a]

[a] *CNRS/ UNIV Pau & Pays Adour, Institut Des Sciences Analytiques et de Physico-Chimie pour l'environnement et les Materiaux –, UMR5254, 64000, Pau, France. Hélioparc Pau Pyrénées 2avenue du Président Angot, 64053 PAU Cedex 09 – France.*

[b]*Department of Physical Chemistry, University of Vigo, Lagoas-Marcosende s/n, 36310.Vigo, Spain*

[c]*Department of Chemistry, University of Patras, GR-26500, Greece*

*corresponding author: panagiotis.karamanis@univ-pau.fr

Abstract.

The synthesis and optoelectronics properties of polyaromatic hydrocarbons (PAHs) doped with boron and nitrogen units (BN) monopolize the interest of increasing numbers of researchers the past few years. The key-concept fueling these attempts lies on the prospect of engineering novel organic compounds of versatile physical and chemical properties using well known all-carbon systems as scaffolds. Among the various BN doped PAHs synthesized so far one could distinguish two categories. The most common one, comprises systems in which BN units replace aromatic CC bonds. The second one, in which this study aims to, refers to systems wherein the BN unit replaces intercyclic CC bonds linking two independent aromatic sextets within the framework of a given PAH. In this work, starting from a reference molecule belonging to the latter category, namely the pyridine-adduct of borazine, we open the subject of polyaromatic hydrocarbons doped with intercyclic boron nitrogen bonds. Our results, based on state of the art ab-initio and DFT wavefunction methods, suggests that intercyclic BN bonds, referred in the literature as "N→B dative bonds", if successfully incorporated to (in)finite polyaromatic sections may alter the optical absorption profiles of the parental systems in a greater extent than typical BN aromatic units. Specifically, we predict and comprehensively interpret the capacity of N→B dative bonds to switch-on extra-strong one- and two-photon quantum transitions followed by intense transfer of charge. The strong excited states alternation triggered by the presence of N→B dative bonds, may unleash exceptionally high non-linear-optical (NLO) optical responses and could find a prosper ground in organic optoelectronic technologies.

1. Introduction

Polyaromatic hydrocarbons (PAHs) doped with one or more B-N units have attracted tremendous attention[1,2,3,4,5,6] in the recent years owed to their potential applications in areas expanding from organic optoelectronics and energy[7,8,9] to molecular biology.[10] The driving scientific hypothesis behind these attempts is that the replacement of a CC bond with a BN unit may alter the electronic structure and electrooptic behavior of the parental system without distorting its spatial structure nor changing its total number of electrons. Therefore, starting from a simple PAH one might fabricate an entirely new chemical space[11] of BN doped isosteres profiting of the available permutations in terms of doping sites and orientation of the embedded units. A representative example can be found in the work of, Liu et al.[12] demonstrating that six BN isosteres of identical planar shape but different optical absorption profiles could be engineered using the molecule of naphthalene as scaffold. Also, very recently Bonifazi and co-workers[13] succeeded in replacing the carbon atoms at the zigzag periphery of a benzo[*fg*]tetracenyl derivative with a "NBN triads" and they demonstrated their potential in forming strong H-bonded complexes.

One of the key molecular properties that should be directly affected from BN doping is the molecular dipole moment. This can be easily understood considering the electronegativity difference between boron and nitrogen which should create a local separation of charge within a given PAH. Therefore, upon BN doping a nonpolar PAH can be immediately converted to a polar molecule preserving its spatial structure and thermodynamic stability. Going a step further, if multi-BN doping[14] is applied, one can potentially tune or cancel the polarity of the final product by controlling the occurring additive effects via the relative orientation of the embedded BN units.

Bearing in mind the Taylor expansion[15,16,17] in **Eq(1)** that describes the induced dipole moment ($\Delta\mu$) of a molecule in the presence of a uniform homogenous static electric field (F), it can be easily deducted that BN doping should impact an entire "ecosystem" of molecular properties widely known as the linear (α) dipole polarizabilities and the first and second dipole hyperpolarizabilities (β, γ).

$$\Delta\mu = \alpha F + \frac{1}{2}\beta F^2 + \frac{1}{6}\gamma F^3 + ... \quad (1)$$

These field dependent molecular properties are of vital scientific and technological importance in the realm of photonics since they govern the non-linear optical behavior of molecules and materials.[18]

Based on the above hypothesis and relying on previous experience in nanographene systems,[19,20,21] in this work we open the subject of the non-linear optical properties of PAHs and nanographenes doped with boron nitrogen dative bonds. A dative bond[22,23] denoted in the literature as D→A, is formed between two fragments, one playing the role of an electron donor (D) and the other role an acceptor (A). In terms of simplified valence bond theory, within a dative bond, the donor atom offers an entire "pair of electrons" to

the occurring bonding while the acceptor contributes with a vacant orbital. The major feature that distinguishes a dative bond from a covalent one is that, upon rupture, the former should preferably yield two neutral species of vanishing spin polarization or in some cases two spin polarized charged species.[22] Instead, a covalent bond should deliver either two spin-polarized fragments or two oppositely charged species. At the atomic level, D→A dative bonds feature stronger polarities and greater lengths than typical covalent bonds, but they are also characterized by lesser stability. Nevertheless, the past decades a series of stable polyaromatic molecules have been successfully synthesized[24,25,16] and studied proving the viability of dative bonds between boron and nitrogen, especially when an N→B unit participates in polyaromatic networks.

Maybe the most representative PAH that accommodates in its framework a N→B bond is the pyridine adduct of borazine (PAB), synthesized as a yellow colored powder few decades ago.[26] In terms of coordination chemistry, PAB is considered as a dative-complex built[27] from borabenzene (acceptor) and pyridine (donor). Such borabenzene-Lewis base adducts,[28,29] in which the boron atom is stabilized by a donor moiety, have proven remarkably interesting because they stabilize borabenzene molecule which has not been observed in free form, up until now. From another point of view, this two-ring simple molecule can be described as an isostere of biphenyl (Ph_2) in which one N→B unit replaces the "single" CC bond that links two heteroaromatic sextets.

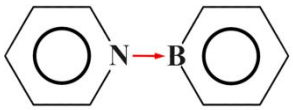

Scheme 1 pyridine - borabenzene adduct

The latter definition is quite handy in the context of this study because we can easily distinguish dative complexes as PAB from other sp^2-type BN/CC isosteres, as azaborine,[30] in which a BN unit replaces an aromatic CC bond. Such "internalized" intercyclic BN units have been successfully incorporated in the framework of other PAHs such as 10a-Aza-10b-borapyrene, a pyrene isostere comprising an "intercyclic BN unit, synthesized by Bosdet et al.[31] As it will be shown in the current proof-of-concept article, intercyclic boron and nitrogen dative bonds when incorporated on a polyaromatic scaffold, may trigger strong charge transfer excited states which, in turn, are translated to exceptionally high non-linear optical responses. The model systems analyzed and discussed in this work comprise either species that have be already synthesized or prototype molecules upon to which novel BN architectures could be engineered if we consider the rapid developments in the field of BN doped polyaromatics.

2. Computational Details

Most computations in finite systems have been carried out with GAUSSIAN 09[32] and GAUSSIAN 16[33] suite of programs. Computations performed in periodic infinite systems and analytical computations of the vibrational contribution on the first dipole hyperpolarizabilities have been conducted with a development version of CRYSTAL 17.[34] The static dipole (hyper)polarizabilities reported in this work have been computed either analytically within the coupled perturbed Hartree-Fock/Kohn-Sham approaches[35,36] (CPHF, CPKS) or via the finite field (FF) approximation (see ref. [37] and references therein). Details about the accuracy thresholds used during the FF computations is provided in supporting material. Bearing in mind that the dynamic electron correlation plays a pivotal role in the determination of linear and nonlinear polarizabilities, for the smallest systems of this study we applied the FF approximation relying on field induced perturbation energies computed with a hierarchy of ab-initio methods comprising the Hartree-Fock (HF) method, second and fourth order Møller-Plesset perturbation theory (MP2, MP4) and the coupled-cluster approximations CCSD and CCSD(T) as implemented in GAUSSIAN software.

The FF approach has been used in the case of all post-HF ab initio methods using the field perturbed energies. DFT property values of α and β have been computed analytically while the DFT second hyperpolarizability values have been obtained from analytical field perturbed analytical first hyperpolarizabilities.[38] Concerning the accuracy of the FF calculations we used convergence criteria and field-strength combinations that reproduce up to an acceptable degree the analytical HF values of the dipole polarizabilities and first hyperpolarizabilities. In the case of N→B systems field-strengths of of 0.002, 0.004 and 0.008 au were used. For all-carbon systems, a combination of slightly stronger fields was applied (0.0025, 0.005 and 0.010 au). At HF level the root mean square (RMS) convergence criterion in GAUSSIAN 09 and 16 were set at 10^{-11} au, (SCF=conver=11) while in CCSD(T) computations an energy convergence criterion of 10^{-9} au (CCSD=conver=9) was imposed.

For the larger systems of this study we mainly relied on two long-range corrected density functional theory (DFT) methods, namely, the Coulomb-attenuating CAM-B3LYP[39] and the long range corrected LC-ωHPBE[40] functionals. In the latter method we have used three different range separating parameters. Specifically, ω=0.4 au^{-1} which is the default value in GAUSSIAN 16, ω=0.3 au^{-1} that in some selected species of this study reproduce up to a great extend excitation energies and transition dipoles obtained with the equation of motion couple-cluster method (EOMCCSD)[41] available in GAUSSIAN 09 and 16, and ω=0.25 au^{-1} which in some species returned hyperpolarizability values close to the MP2 approximation. Benchmark (hyper)polarizability calculations using other pure and hybrid functionals are provided in supporting material including calculations performed with the double hybrid functionals BP2BLYP[42] and PBEQIDH[43]. Spectroscopic properties, excitation energies, transition dipole moments, and excited state dipole moments have been computed using either the configuration interaction singles (CIS) or by applying

the time-dependent DFT approximation (TD-DFT). In some of the molecules considered, the required transition dipole moments between excited states have been computed with MULTIWFN program,[44] which at the CIS level of theory reproduces the transition dipole obtained with GAUSSIAN 09 and 16. Charge transfer excited states have been analyzed by means of electron density differences between excited states and/or natural transition orbitals[45,46,20] (NTOs) in terms of "excited particle" to "empty hole" of the electronic transition density matrix. Intrinsic atomic polarizabilities ($\overline{\alpha}^{intr}$) and mean intrinsic polarizability densities (MIPD) used in this work have been computed within the Fractional Occupation Hirsfeld-Iterative (FOHI) partitioning scheme (see refs [47, 48], and references therein). As explained elsewhere,[49] the term "intrinsic atomic polarizability" refers to the origin-independent contribution of each atom to the molecular polarizability. The delocalization indices (*n*-Dis) accounting for the multicenter electron delocalization and aromaticity[50] were obtained following a QTAIM-based scheme implementation via the Generalized Population Analysis (GPA).[51] A more detailed discussion including the Quantum Theory of Atoms In Molecules (QTAIM) implementation can be found in references [52 and 53]. Implementation details of the latter method can be found in the supporting information of Ref [21] and applications in doped graphene in Ref [54], respectively. Finally, definitions of the scalar quantities, namely, the mean (or average) static dipole polarizability ($\overline{\alpha}$), the total first order hyperpolarizability (β_{tot}) and the average second hyperpolarizability ($\overline{\gamma}$) considered in this work are given below in terms of tensor Cartesian components α_{ij}, β_{ijk}, and γ_{ijkl}:

$$\overline{\alpha} = \frac{1}{3}\left(\alpha_{xx} + \alpha_{yy} + \alpha_{zz}\right) \quad (2)$$

$$\beta_{tot} = \left(\left(\beta_{xxx} + \beta_{xyy} + \beta_{xzz}\right)^2 + \left(\beta_{yxx} + \beta_{yyy} + \beta_{yzz}\right)^2 + \left(\beta_{zxx} + \beta_{zyy} + \beta_{zzz}\right)^2\right)^{1/2} \quad (3)$$

$$\overline{\gamma} = 1/5\left(\gamma_{xxxx} + \gamma_{yyyy} + \gamma_{zzzz} + 2\gamma_{xxyy} + 2\gamma_{yyzz} + 2\gamma_{xxzz}\right) \quad (4)$$

3. Results and Discussion

The molecular structure of PAB, belonging to the C_2 point group, is shown in **Fig. 1(a)**. Molecules of such symmetry[15] bear one independent component of the dipole moment along the C_2 symmetry axis, four nonvanishing components of the first hyperpolarizability and nine components of the second dipole hyperpolarizability γ. In **Fig. 1(b)** we illustrate PAB's MIPDs together with the corresponding isotropic (mean) intrinsic atomic polarizabilities ($\bar{\alpha}^{intr}$) and the computed *6*-Dis for each ring. In terms of π-electron ring delocalization in the two heteroaromatic rings, we see that out of the two fragments, pyridine is the most delocalized one featuring the largest *6*-Dis (7.8 au vs 5.9 au). At the same level of theory, the computed *6*-Dis value of 8.0, of its all carbon analogue, namely, the molecule of biphenyl (Ph_2), suggest that that π-electron network of pyridine should be practically as delocalized as in Ph_2, and thus almost equally aromatic. On the other hand, borabenzene fragment appears considerably less delocalized, and thus, less aromatic. The evident differences in delocalization between the two fragments of PAB is in accord with the illustrated MIPD topologies that has been shown to reproduce the aromaticity patterns in polyaromatic hydrocarbons and graphene molecules[49]. Hence, while in pyridine we observe a continuous circular area of high densities, in the case of borabenzene this feature is suppressed in the vicinity of boron atom.

In **Fig. 1(c),** we show the intrinsic polarizabilities of PAB's constituent fragments, namely, pyridine and borabenzene. A careful comparison between these values and those corresponding to PAB reveals that the molecular $\bar{\alpha}^{intr}$of PAB, defined as the sum of all atomic contributions without taking into account charge transfer interactions[47,48], is found to be considerably smaller than the sum of the intrinsic molecular polarizabilities of the free systems. This trend is in line with the minimum polarizability principle[55,56] introduced few decades ago suggesting that "the natural direction of evolution of any system is toward a state of minimum polarizability". In the current case, out of the two PAB's fragments, the less affected one is borabenzene which appears to be only 5% less polarizable after the formation of the BN bond. On the other hand, pyridine fragment, in PAB, experiences an overall polarizability decrease of 18% with respect to its free form. Out of the eleven PAB's heavy atoms, the most affected one is the atom of N which undergoes a massive polarizability decrease of about 75% as compared to free pyridine. Hence, while N[$\bar{\alpha}^{intr}$] is larger than B[$\bar{\alpha}^{intr}$] in free pyridine and borabenzene fragments, respectively, in their dimer form, nitrogen becomes the least polarizable heavy atom of the whole molecule and two times less polarizable than boron. The observed trend is in accord with the general intuitive understanding of dative N→B bonds that imply a "direct transfer of electron density" from N to B. As we will see in the next few pages, the "excess" electron density accumulated in borabenzene after the dimer formations is of pivotal importance for the first and second hyperpolarizabilities of N→B doped PAHs.

In **Table I** we have summarized the dipole (hyper)polarizabilities of PAB computed at several levels of theory, using as reference a fully optimized nuclear geometry determined with the MP2(FULL)/6-311+G(2d,2p) method. At the respective level of theory we obtained a B-N distance of 1.5415 Å, which is very close to the experimental[22] B-N distance of 1.558 Å that has been observed in the corresponding monocrystal and represents a typical length of a N→B dative bond. A first glance on the data of **Table I** confirms that PAB is a strongly polar molecule characterized by sizable NLO response owed to the presence of the N→B embedded dative bond. In physics convention the observed negative sign of μ_z implies that for the molecular orientation shown in **Fig. 1,** the dipole moment vector should point from borabenzene fragment to pyridine. The obtained dipole moment of PAB at CCSD(T), MP2 and MP4 levels, reaches the value of 3.2 au (8.1 D) with either basis set in both optimized geometries.

Out of the various approximations considered MP2, MP4 and CAM-B3LYP methods follow closely the results obtained at the CCSD(T) level converging to the value of 6.9×10^3 au. The sign of β, which is opposite to the sign of the ground state dipole moment for the considered molecular orientation (see **Fig. 1**), indicates that the underlying charge transfer mechanism should involve electron migration to the opposite direction of the ground state dipole moment. In addition, we have computed the vibrational contributions[57] on the static first and second dipole hyperpolarizability at an infinite optical frequency wavelenght at the CAM-B3LYP/6-311+G(2d,2p) level of theory using CRYSTAL 17. The obtained outcomes suggest that one should expect about 25% and 50% increased values for the dominant components of β and γ, respectively, (see **Table S4**) most likely owed to the ionic character on the N→B dative bond. Hence, at the respective level of theory the total first hyperpolarizability ($\beta^{tot}=\beta^{e}+\beta^{vib}$) along the dipole moment axis raises to 7.7×10^3 au from 6.2×10^3 au (β^{e}). On the other hand, the corresponding component of theintensity-dependent refractive index (IDRI)[58] total fist hyperpolarizability ($\gamma^{tot}=\gamma^{e}+\gamma^{vib}$) is found about 1.2×10^6 au, while γ^{e} along this direction amounts to 0.8×10^6 au. Note that the respective values correspond to a CAM-B3LYP/6-311+G(2d, 2p) optimized geometry which is slightly different than the one used in **Table I**. Unfortunately, no experimental (hyper)polarizability data are available to make the appropriate comparisons. Therefore, for the reference molecule of PAB the CCSD(T)/6-311+G(2d,2p) results reported in the current study provide the best estimation of the dipole moment and dipole (hyper)polarizabilities reported so far. More discussion and results about the method dependence of these properties is provided as supporting material.

Comparisons between the (hyper)polarizabilities of PAB and bi-phenyl (Ph_2) are given 6in **Table II**. A prompt study of the obtained property values reveals that the respective type of N→B substitution, apart from triggering a strong first hyperpolarizability, it has dramatic effect on γ stemming mainly from the γ_{zzzz} axial component. The largest increase ratios (~10) are predicted at the MP2 and CCSD(T) levels of theory. On the other hand, the CCSD, LC-ωHPBE and CAM-B3LYP methods yielded increase ratios between 7.3

and 8. We further analyzed the charge transfer mechanism responsible for the large first and second order NLO responses of PAB via the two and three level sum-over-states (SOS) models[59,60]. Within this approach, we computed the most dominant off-resonant longitudinal components (β_{zzz} and γ_{zzzz}) of PAB using the following truncated expressions that have been proven quite handy in the case of a vast assortment of organic chromophores reported in the literature[59].

$$\beta_{zzz}^{2\text{state}} = 6\frac{M_{ge}^2 \Delta\mu_{ge}}{E_{ge}^2} \quad (5)$$

$$\gamma_{zzzz}^{3\text{state}} = \underbrace{24\frac{M_{ge}^2 \Delta\mu_{ge}^2}{E_{ge}^3}}_{\text{Dipolar}} \underbrace{-24\frac{M_{ge}^4}{E_{ge}^3}}_{\text{Negative}} + \underbrace{24\sum_{e'}\frac{M_{ge}^2 M_{ee'}^2}{E_{ge}^2 E_{ge'}}}_{\text{Two Photon}} \quad (6)$$

In the above equations $M_{g(e,e')}$ represent the transition dipoles between the ground state (g) and the accessible singlet excited states (e, e′). $E_{g(e,e')}$ stand for the corresponding excitation energies while $\Delta\mu_{ge}$ is the dipole moment difference between the ground (g) and excited state (e) along the z axis. **Eq. (6)** involves transition between at least three states and it is composed by three terms. Specifically, the "Dipolar" term depends on the first dipole hyperpolarizability and it appears only in non-centrosymmetric molecules as PAB for which $\Delta\mu_{ge} \neq 0$. The "Negative" term, on the other hand, in the rare cases that becomes dominant is associated to negative second hyperpolarizabilities which in turn are related to negative refractive indexes and laser beam self-defocusing effects. The third and last term referred as "two photon term" represents contributions from higher excited states (e′) that should be coupled with the excited state (e) via non-zero transition moments M_{ee}.

Based on the above expression we identified and plotted in **Fig. 2(a)** the optical paths that govern, up to a great extent, PAB's hyperpolarization mechanism within its first 100 states. For this task, we used the LC-ωHPBE$^{\omega=0.3}$ long range corrected functional which returned excitation energies and transition dipoles close to those obtained at the EOM-CCSD/6-311+G(2d,2p) level of theory. A detailed analysis of these data is provided as supporting material where we also provide a discussion of the most important optical paths in the case of Ph_2. Here we will only mention that PAB owes its enhanced NLO properties solely to one quantum transition occurring between its ground and first excited state ($S_0 \rightarrow S_1$). This excitation yields a pronounced $\Delta\mu$ difference of 4.353au stemming from an intense transfer of charge opposite to the molecular dipole. This is readily seen in the natural transition orbital topologies, drawn in the top of **Fig. 2(a)**, which clearly imply a coherent π-π* density shift from borabenzene fragment to pyridine. As mentioned earlier, upon excitation the latter fragment behaves as strong electron donor using the excess electron density received from pyridine during the formation of the dimer. A closer look at the computed values of each term of **Eq. (6)**, shown at the bottom of **Fig. 2(a),** exposes that the transition $S_0 \rightarrow S_1$ not

only governs the overall size of β but also renders the dipolar term as the most dominant one out of the three we have inserted in **Eq. (6)**. Bearing in mind that symmetry restrictions cancel the contribution of the later one-photon term in the case of its parental all-carbon analogue (Ph_2), one could safely conclude that the enhanced second hyperpolarizability of PAB should be exclusively attributed to one-photon excitations fueled by the polar nature of the N→B dative bond. The latter deduction, relating the large hyperpolarizabilities of PAB with particular features of N→B dative bond, is fully verified by the outcomes presented in **Fig. 2(b)** where we see that N→B unit sparks, by far, the largest first and second NLO responses among all possible isomers of BN doped Ph_2.

Relying on the insights gained in the previous section, to investigate the impact of a dative N→B bond in the first hyperpolarizability of larger polyaromatic architectures, we considered hexa-peri-hexabenzocoronene (HBC) which is a reference all-benzenoid[61] simple molecular graphene. This "discotic" hexagonal PAH, built from six fused aromatic benzene rings, has attracted lots of interest owed to its capacity to form columnar hyper-structures and liquid crystals with potential applications in organic electronics.[62] Among the abundant functionalized HBC's derivatives that can be fabricated through well-established synthetic protocols,[63] we chose a rather simple version bearing one biphenyl molecule attached in one of its six axial terminal aromatic sextets in ortho-position (see **Fig. 3)**. Using this functionalized HBC nanographene (hereafter Ph_2HBC) as doping substrate, we replaced four intercyclic carbon-carbon bonds (one at a time) with a BN unit creating four doped isosteres, Ph_2HBC-(1, 2, 3, 4). The common structural feature in these systems is that in each case, B and N atoms participate in different aromatic sextets, which are located a) inside the graphene core, b) at the HBC-Ph_2 heterojunctions and c) in the middle of the two external benzene rings.

The first dipole hyperpolarizabilities along the C_2 symmetry axis ($\beta_{\parallel}$) of all Ph_2HBC isosteres are contrasted at different levels of theory in **Fig. 3(a)**. A quick glance on the illustrated results reveals two dominant trends. The first concerns the strong effect of doping on β since all doped systems exhibit larger hyperpolarizabilities than the pristine Ph_2HBC. As a result, even the least hyperpolarizable out of the four trial models considered, namely structure Ph_2HBC-4, is characterized by a static first hyperpolarizability which lies 17 times higher than in its parent structure (3.6×10^2 vs 6.1×10^3 au) at MP2 level of theory. The second and most intriguing trend, manifests by the impressive dependence of β on the doping site. As seen, when the BN unit replaces external CC intercyclic bonds, extra strong first order NLO responses are delivered. On the other hand, when the BN unit is inserted between the internal aromatic sextets of HBC the first dipole hyperpolarizabilities considerable decrease. The largest hyperpolarizability enhancement is observed in Ph_2HBC-**2** where the BN unit is placed in the heterojunction between biphenyl and HBC. At

the MP2 level of theory it is suggested that Ph_2HBC-**2's** β lies two orders of magnitude higher than its all-carbon-analogue.

Turning our attention to the dependence of β on the method applied, it becomes evident that electron correlation correction, defined as β^{MP2}-β^{HF}, reaches a sharp pick in the most hyperpolarizable isostere, namely, Ph_2HBC-**2**. The main trend that characterizes the observed method performance suggests that the larger the first dipole hyperpolarizability is, the stronger the deviations between the DFT functionals become. Specifically, while for structures **1** and **2** CAM-B3LYP overshoots the MP2 values, in the case of the structures **3** and **4** the latter functional yields β values bracketed between HF and MP2, lying closer to the former. LC-ωHPBE, on the other hand, follows a more consistent behavior yielding β values between the HF and MP2 limits for all species. Interestingly, even if we choose a range separating parameter (ω=0.25 au^{-1}) that practically reproduces the MP2 outcomes in the most hyperpolarizable species **1** and **2**, we see that this has a limited effect in the case of the internally graphene doped models. Such method trends most likely originate from some notable and intriguing difference between certain bonding features related to the BN unit between **(1**, **2**) and (**3** ,**4**) isomers, that deserve to be investigated in more depth.

The observed β variations should primarily come from the different degree of charge transfer upon electronic excitations between the various isosteres and secondarily from the band gap narrowing in the case of systems **1** and **2**. This is, at least, what **Fig. 3(b)** suggests, where we have plotted the evolution of the corresponding $\Delta\mu$ values and energy differences (ΔE) of the most intense charge transfer transition for each isostere. As it is readily seen, the strong correlations between the magnitude of β and the N→B position follow closely the computed differences between the ground and the first symmetry allowed charge transfer state in all doped Ph_2HBC systems. Chemical intuition suggests that the reduced capacity of BN doped Ph_2HBC-**3** and **-4** species to stimulate intense charge transfer excited states should be associated to the loss of BN bond's dative character after its incorporation in the network of the HBC fragment. Bearing in mind that a N→B dative bond is longer than a typical covalent bond the previous deduction is indirectly supported by the computed BN bond lengths shown in **Fig. 3(b)**. Specifically, in Ph_2HBC(3,4) species the BN bonds (~1.45 Å) are notably shorter than in a in Ph_2HBC-(1,2) (~1.52 Å) and free PAB (~1.52 Å), respectively.

To better rationalize the relevance of the above observation, we focused our computational efforts on BN-doped pyrene[31] (hereafter BNPYR) that can be identified as a local structure in both Ph_2HBC-(3,4) species (**Fig. 4**). From another point of view, BNPYR can be considered as a derivative of PAB functionalized with two HC=CH units that bridge its heteroaromatic sextets. Referred in the literature[64] as a "K-region", the latter structural unit is known[65] for its strong effect on the electronic structure of nanographenes. Indeed, **Fig. 4** exposes that the first hyperpolarizabilities of PAB and BNPYR follow the same trend as in the case of the BN doped Ph_2HBC series. The key idea to understand the observed strong

dip in β ($7.9\times10^3 \rightarrow 1.6\times10^3$ au) between the two derivatives of pyrene was found after we saturated the two K-regions with hydrogens. Such a trivial chemical modification increased the distance of the BN bond and strengthened its polarity. In addition, a sharp hyperpolarizability increase from 1.3×10^3 to 5.5×10^3 au is delivered, without lowering considerably the molecular bandgap.

The role of the K-region π-bonds can be better understood if we compare the MIP density topologies and delocalization profiles between these pyrene derivatives. As seen in **Fig. 5,** hydrogen saturation has a dramatic impact on the "non-aromatic" hexagons, formed by the incorporation of the two K-regions in PAB which become 13 times less delocalized (1.3 → 0.1) upon hydrogen saturation. This is expected to limit the interaction between the two K-regions via the so called "mesomeric effects" which in the case of BNPYR should implicate the π-bonding of the two HC=CH bridging units. Without any significant electron delocalization in this part of the molecule, charge transfer interactions between the two heteroaromatic rings are expected to be stronger in saturated BNPYR than in its unsaturated analogue.

If, now, we revisit the MIP density topologies and delocalization profiles of PAB, we shall see that hydrogen saturation restores a considerable portion of the changes brought by the insertion of the two K-regions. Specifically, while in PAB the average delocalization of the heteroaromatic ring is at 6.9 au, after the incorporation of the two K-regions this value reduces to 2.8 before it raises back to 5.0 au upon hydrogen saturation. In such a manner, borabenzene's electron accepting (donating) strength in the ground (excited) states, is expected to recover up to a great extent. Therefore, saturated BNPYR could be alternatively considered as an aromatic hydrocarbon doped with one N→B dative bond. This last deduction, fits well to the similar variation of β observed between PAB and saturated (N→B)PYR at the CCSD and CCSD(T) levels ($\beta^{CCSD}<\beta^{CCSD(T)}$), which, in turn, contrasts the one we observe in BNPYR ($\beta^{CCSD}>\beta^{CCSD(T)}$). Furthermore, calculated B-N bond orders of the three systems shown in **Fig. 4** reveal that while in BNPYR boron nitrogen bond features a bond order of 1.00 au, in saturated BNPYR and PAB the computed bond orders lie considerably lower, at 0.89 and 0.84 au, respectively.

The dative bonding character of BN unit in BNPYR is further justified by the computed NTO transition orbitals, shown in **Fig. 5.** As it can be seen**,** the underlying quantum transition clearly involves an unambiguous density shift between the two heteroaromatic hexagons matching the one identified in PAB. On the other hand, BNPYR's NTO topologies expose a strong contribution of the two K-region that disperse the excited density shifts across the whole body of the system. Thus, the probability of strong dipole moment differences between its ground and the most intense excited state is largely reduced.

The above analysis not only explains the anomalous hyperpolarizability evolution observed in the case of the doped Ph_2HBC series but brings to light an effective designing strategy. Specifically, one can

significantly enhance the first order NLO response of a given polyaromatic hydrocarbon doped with intercyclic BN bonds simply by activating the "dative character" of the embedded BN unit. A demonstration of this concept applied in two nanographenes is illustrated in **Fig. 6**. Specifically, upon hydrogen passivation the first hyperpolarizability of the doped ribbon increases by a factor of two, while, in the case of the star-shape graphene flake comprising six internal BN heterocyclic bonds, an impressive increase of one order of magnitude is delivered.

To investigate the effect of N→B dative bonds on the second dipole hyperpolarizability of nanographenes, we have designed the series of models depicted in **Fig. 7(a),** namely, $C_{138}(N\rightarrow B)_6X$ and $C_{138}(BN)_6X$ (where X=H, -Ph≡-C_6H_5). Either group of models have been built upon the same edge-functionalized pristine nanographene, designated as $C_{150}X$. The common feature between $C_{138}(N\rightarrow B, BN)_6X$ models is that six BN units replace an equal number of CC bonded pairs creating four different isosteres. In the first group, denoted with {N→B}, the incorporated units substitute single CC bonds connecting the terminal diagonal aromatic sextets with the functionalization groups. In the second set of systems, labeled with {BN}, six BN units replace aromatic CC bonds of the peripheral aromatic sextets of the graphene core. In all cases the incorporated N→B and BN units were fixed in a centrosymmetric fashion that induce the lowest possible molecular polarization to the ground state of the doped systems.

The optical absorption profiles of two of the above isosteres are illustrated in **Fig. 7(b)** within a spectral window between 0 to 6 eV. As seen, while aromatic BN doping brings a rather weak change on the absorption outline of its pristine counterpart, intercyclic N→B substitution results to an extraordinarily different UV-VIS spectrum characterized by an additional absorption pick lying lower in energy. In **Fig. 7(c)**, where we have drawn their spectral evolution with respect to the number of intercyclic BN units, it is immediately seen that the position and the intensity of the latter absorption band is controlled by the number of the incorporated N→B dative bonds. Hence, while the absorption profile of $C_{138}(N\rightarrow B)_{n=1}X$ is similar to the one of its parent flake, it gradually transforms to the final two-peak absorption spectrum as the number of the incorporated N→B units increases.

In **Table III** we have summarized HOMO-LUMO gaps (HLG), vertical excitation energies $E_{\lambda max}$, and mean dipole (hyper)polarizabilities of all the systems presented in **Fig. 7**. As its readily seen, N→B doping induces smaller HLG and $E_{\lambda max}$ excitation energies, larger dipole polarizabilities and vastly amplified second-order non-linear responses. In some cases, the hyperpolarizabilities of the N→B doped systems appear to be 510% and 950% larger than the hyperpolarizabilities of the parental all-carbon nanographenes depending on the X functional groups. On the other hand, BN aromatic substitutions bring considerably modest property changes as we previously witnessed in the case of BN doped Ph_2. For instance, while the average hyperpolarizability of $C_{150}Ph$, at the specific level of theory, reaches a value of 0.9×10^7 au, upon

N→B doping it "skyrockets" to 1.0×10^8 au. More calculations addressing the influence of the DFT method used on the hyperpolarizabilities of these is provided in supporting material.

As mentioned earlier, one photon optical paths do not affect the overall first and second hyperpolarizabilities of centrosymmetric molecules because, in principle, the symmetry allowed vertical, nonresonant, excitations lead to symmetric electron density shifts, and thus, to nonpolar excited states. Therefore, the large NLO responses computed for the above species should be solely attributed to optical channels implicating at least three low lying excited states that should be bound by strong $M_{ee'}$ transition dipoles. In terms of the SOS model applied earlier, the latter deduction brings forth that out of the three terms of **Eq. 3** the large second hyperpolarizabilities of these species should be triggered strictly by quantum transitions included in the two-photon term. A representative example of the charge transfer process involved in such two photon interaction is given in supporting material by means of electron density differences and attachment/detachment density[66] plots.

We will end this report with a brief discussion of size effects on the first dipole hyperpolarizability obtained in a series of doped flakes of increasing size. The acquired outcomes, depicted in **Fig. 8(a),** point out that as the size of the graphene core increases the effect of intercyclic BN substitution should considerably weaken. Hence, while in a small functionalized graphene flake built from 48 carbon atoms, as HBC, the increase in the second hyperpolarizability reaches a factor of 20 to 31, as we go to larger functionalized nanographenes (e.g. built from 222 carbon atoms) the specific effect considerably fades. Given that the second hyperpolarizability of molecules depend on the total number of their electrons,[60] the observed size effect point out that N→B doping could prove as a more effective strategy in small nanographenes systems, which in addition are easier to access and/or modify via current synthetic strategies. A convincing example of this effect is shown in **Fig.8 (b),** where we see that two N→B functionalized graphenes built from 48 and 114 carbon atoms are predicted to be more hyperpolarizable than a large functionalized pristine flake of 222 carbon atoms. Interestingly, the static first hyperpolarizabilities obtained for the smallest member of these species is about one order of magnitude larger than in oxygen doped graphene type hydrocarbons of similar size that has been synthesized and studied theoretically and experimentally by Miletić *et al.* [67] few years ago. Specifically, in this work the largest reported first static hyperpolarizability at the CAM-B3LYP/6-31+G(d) was found about 1.8×10^6 au while at the same level of theory with a larger basis set (6-311G(d)) the computed second hyperpolarizability of the HBC derivative shown in **Fig. 8 (b)** lies considerably higher, at 5.5×10^7 au.

The revealed trends obtained in finite graphene sections have been extended to the periodic graphene ribbon of infinite length shown in **Fig. 9**. The hyperpolarizability outcomes listed in that figure confirm that N→B dative bonds, when incorporated in a narrow graphene ribbon, might amplify its second order

responses even by an order of magnitude without considerably reducing its band gap, that in some application may be considered as an important limiting factor connected to laser-induced damage thresholds.[68] What's more, it is interesting to stress that the respective increase is achieved along the finite in plane spatial direction of the ribbon. This is a noteworthy outcome pointing out an effective strategy that would allow to take full advantage of the finite spatial direction ion graphene ribbons providing, in such a manner, additional practical solutions in terms of their possible implementation in functional NLO devices.

4. Conclusions

In this work we have investigated the (non)linear optical properties of polyaromatic hydrocarbons with fused N→B "dative bonds" using state of the art in ab-initio and DFT methods. Our results suggest that N→B dative bonds formed between borabenzene and pyridine when incorporated to either small PAHs or (in)finite graphene sections bring considerably drastic changes on the linear and nonlinear profiles of the parental systems. Particularly, our computational outcomes predict that N→B dative bonds may increase the first and second hyperpolarizability of a given PAH even by an order of magnitude when incorporated to its structure. Excited state analysis performed within the TD-DFT and CIS frameworks revealed that the observed changes originate from strong charge transfer excited states triggered by the fused borabenzene rings. The dominant charge transfer mechanism explaining the enhanced NLO responses in those systems resembles the one identified in conventional push-pull chromophores extensively studied[18] in the past with respect to their NLO properties. Furthermore, the difference between intercyclic BN and N→B bonds fused in nanographene have been identified, analyzed, and explained. Finally, it is demonstrated how one could control the character of a BN bond, incorporated in the framework of a PAH, by reducing the delocalization of the surrounding CC bonds.

5. Acknowledgments

Part of this work was granted access to the HPC resources of [CCRT/CINES/IDRIS] under the allocation 2019-2020 [A0040807031] made by GENCI (Grand Equipement National de Calcul Intensif). We also acknowledge the "Direction du Numérique" of the "Université de Pau et des Pays de l'Adour" and the mésocentre Aquitain (MCIA) for the computing facilities provided. H.D. thanks ANR for the one-year postdoc position in project FOIST and N.O.M. thanks "Xunta de Galicia" for a postdoctoral contract.

6. Supporting Information

In Supporting Information, we provide a) additional data concerning the hyperpolarizabilities of **PAB** computed at various levels of theory. b) a detailed comparison between the excitation channels of **PAB** and $\mathbf{Ph_2}$. c) The influence of the method used on the effects the hyperpolarizabilities of intra and inter BN doped graphene systems. d) A visual description of photon interaction in (NB) functionalized graphenes. e) detailed data concerning the vibrational contributions on the static first and second dipole hyperpolarizability.

References

[1] Wang, X.-Y.; Zhuang, F.-D.; Wang, R.-B.; Wang, X.-C.; Cao, X.-Y.; Wang, J.-Y.; Pei, J. A Straightforward Strategy toward Large BN-Embedded π-Systems: Synthesis, Structure, and Optoelectronic Properties of Extended BN Heterosuperbenzenes. *J. Am. Chem. Soc.* **2014**, *136* (10), 3764–3767.

[2] Wang, X.-Y.; Wang, J.-Y.; Pei, J. BN Heterosuperbenzenes: Synthesis and Properties. *Chem. Eur. J.* **2015**, *21* (9), 3528–3539.

[3] Giustra, Z. X.; Liu, S.-Y. The State of the Art in Azaborine Chemistry: New Synthetic Methods and Applications. *J. Am. Chem. Soc.* **2018**, *140* (4), 1184–1194.

[4] Campbell, P. G.; Marwitz, A. J. V.; Liu, S.-Y. Recent Advances in Azaborine Chemistry. *Ang. Chem. Int. Ed.* **2012**, *51* (25), 6074–6092.

[5] Helten, H. B=N Units as Part of Extended π-Conjugated Oligomers and Polymers. *Chem. Eur. J.* **2016**, *22* (37), 12972–12982.

[6] Chen, Y.; Chen, W.; Qiao, Y.; Lu, X.; Zhou, G. BN-Embedded Polycyclic Aromatic Hydrocarbon Oligomers: Synthesis, Aromaticity, and Reactivity. *Angew. Chem. Int. Ed.* **2020**, *59* (18), 7122–7130.

[7] Campbell, P. G.; Zakharov, L. N.; Grant, D. J.; Dixon, D. A.; Liu, S.-Y. Hydrogen Storage by Boron−Nitrogen Heterocycles: A Simple Route for Spent Fuel Regeneration. *J. Am. Chem. Soc.* **2010**, *132* (10), 3289–3291.

[8] Zeng, T.; Mellerup, S. K.; Yang, D.; Wang, X.; Wang, S.; Stamplecoskie, K. Identifying $(BN)_2$-Pyrenes as a New Class of Singlet Fission Chromophores: Significance of Azaborine Substitution. *J. Phys. Chem. Lett.* **2018**, *9* (11), 2919–2927.

[9] Huang, J.; Li, Y. BN Embedded Polycyclic π-Conjugated Systems: Synthesis, Optoelectronic Properties, and Photovoltaic Applications. *Front. Chem.* **2018**, *6*.

[10] Knack, D. H.; Marshall, J. L.; Harlow, G. P.; Dudzik, A.; Szaleniec, M.; Liu, S.-Y.; Heider, J. BN/CC Isosteric Compounds as Enzyme Inhibitors: N- and B-Ethyl-1,2-Azaborine Inhibit Ethylbenzene Hydroxylation as Nonconvertible Substrate Analogues. *Ang. Chem. Int. Ed.* **2013**, *52* (9), 2599–2601.

[11] Chakraborty, S.; Kayastha, P.; Ramakrishnan, R. The Chemical Space of B, N-Substituted Polycyclic Aromatic Hydrocarbons: Combinatorial Enumeration and High-Throughput First-Principles Modeling. *J. Chem. Phys.* **2019**, *150* (11), 114106.

[12] Liu, Z.; Ishibashi, J. S. A.; Darrigan, C.; Dargelos, A.; Chrostowska, A.; Li, B.; Vasiliu, M.; Dixon, D. A.; Liu, S.-Y. The Least Stable Isomer of BN Naphthalene: Toward Predictive Trends for the Optoelectronic Properties of BN Acenes. *J. Am. Chem. Soc.* **2017**, *139* (17), 6082–6085.

[13] Tasseroul, J.; Lorenzo-Garcia, M. M.; Dosso, J.; Simon, F.; Velari, S.; De Vita, A.; Tecilla, P.; Bonifazi, D. Probing Peripheral H-Bonding Functionalities in BN-Doped Polycyclic Aromatic Hydrocarbons. *J. Org. Chem.* **2020**, *85* (5), 3454–3464.

[14] Wang, X.-Y.; Zhuang, F.-D.; Wang, X.-C.; Cao, X.-Y.; Wang, J.-Y.; Pei, J. Synthesis, Structure and Properties of C3-Symmetric Heterosuperbenzene with Three BN Units. *Chem. Commun.* **2015**, *51* (21), 4368–4371.

[15] Buckingham, A. D. Permanent and Induced Molecular Moments and Long-Range Intermolecular Forces. In *Adv. Chem. Phys.*; Hirschfelder, J. O., Ed.; John Wiley & Sons, Inc., 1967; pp 107–142.

[16] McLean, A. D.; Yoshimine, M. Theory of Molecular Polarizabilities. *J. Chem. Phys.* **1967**, *47* (6), 1927–1935.

[17] *Nonlinear Optics* Boyd, R.W. Academic Press, New York. Pyatt, R. D. 1992.

[18] *Non-Linear Optical Properties of Matter: From Molecules to Condensed Phases*; Papadopoulos, M. G., Sadlej, A. J., Leszczynski, J., Eds.; Challenges and Advances in Computational Chemistry and Physics; Springer Netherlands, 2006.

[19] Otero, N.; Karamanis, P.; El-Kelany, K. E.; Rérat, M.; Maschio, L.; Civalleri, B.; Kirtman, B. Exploring the Linear Optical Properties of Borazine (B3N3) Doped Graphenes. 0D Flakes vs 2D Sheets. *J. Phys. Chem. C* **2017**, *121* (1), 709–722.

[20] Karamanis, P.; Charistos, N. D.; Sigalas, M. P.; Rérat, M. Polyaromatic Systems Combining Increasing Optical Gaps and Amplified Nonlinear Optical Properties. A Comprehensive Theoretical Study on B3N3 Doped Nanographenes. *J. Phys. Chem. C* **2019**, *123* (34), 21135–21149.
[21] Karamanis, P.; Otero, N.; Pouchan, C. Unleashing the Quadratic Nonlinear Optical Responses of Graphene by Confining White-Graphene (h-BN) Sections in Its Framework. *J. Am. Chem. Soc.* **2014**, *136* (20), 7464–7473.
[22] Haaland, A. Covalent versus Dative Bonds to Main Group Metals, a Useful Distinction. *Angew. Chem. Int. Ed. Engl.* **1989**, *28* (8), 992–1007.
[23] Pupim, C. F.; Catão, A. J. L.; López-Castillo, A. Boron–Nitrogen Dative Bond. *J. Mol. Model.* **2018**, *24* (10), 283.
[24] Bosdet, M. J. D.; Piers, W. E. B-N as a C-C Substitute in Aromatic Systems. *Can. J. Chem.* **2009**, *87* (1), 8–29.
[25] Hoic, D. A.; Wolf, J. R.; Davis, W. M.; Fu, G. C. Chemistry of Borabenzene: Efficient and General Synthesis of New Neutral Borabenzene−Ligand Complexes. *Organometallics* **1996**, *15* (4), 1315–1318.
[26] Boese, R.; Finke, N.; Henkelmann, J.; Maier, G.; Paetzold, P.; Reisenauer, H. P.; Schmid, G. Synthese und Strukturuntersuchung von Pyridin-Borabenzol und Pyridin-2-Boranaphthalin. *Chem. Ber.* **1985**, *118* (4), 1644–1654.
[27] Mbarki, M.; Oettinghaus, M.; Raabe, G. Quantum-Chemical Ab Initio Calculations on the Donor–Acceptor Complex Pyridine–Borabenzene (C_5H_5N–BC_5H_5). *Aust. J. Chem.* **2014**, *67* (2), 266.
[28] Zheng, X.; Herberich, G. E. Borabenzene Derivatives. 33. 3,5-Dimethylborabenzene 1,3,4,5-Tetramethylimidazol-2-Ylidene: The First Carbene Adduct of a Borabenzene [1]. *Organometallics* **2000**, *19* (19), 3751–3753.
[29] Légaré, M.-A.; Bélanger-Chabot, G.; De Robillard, G.; Languérand, A.; Maron, L.; Fontaine, F.-G. Insights into the Formation of Borabenzene Adducts via Ligand Exchange Reactions and TMSCl Elimination from Boracyclohexadiene Precursors. *Organometallics* **2014**, *33* (13), 3596–3606.
[30] Marwitz, A. J. V.; Lamm, A. N.; Zakharov, L. N.; Vasiliu, M.; Dixon, D. A.; Liu, S.-Y. BN-Substituted Diphenylacetylene: A Basic Model for Conjugated π-Systems Containing the BN Bond Pair. *Chem. Sci.* **2012**, *3* (3), 825–829.
[31] Bosdet, M. J. D.; Piers, W. E.; Sorensen, T. S.; Parvez, M. 10a-Aza-10b-Borapyrenes: Heterocyclic Analogues of Pyrene with Internalized BN Moieties. *Ang. Chem. Int. Ed.* **2007**, *46* (26), 4940–4943.
[32] Frisch, M. J.; Trucks, G. W.; Schlegel, H. B.; Scuseria G. E; Robb, M. A.; Cheeseman, J. R.; Scalmani, G.; Barone, V.; Mennucci, B.; Petersson, G. A.; *et al. Gaussian 09*, Revision D.01; Gaussian, Inc., Wallingford CT, **2009**.
[33] Frisch, M. J.; Trucks, G. W.; Schlegel, H. B.; Scuseria, G. E.; Robb, M. A.; Cheeseman, J. R.; Scalmani, G.; Barone, V.; Petersson G. A.; *et al. Gaussian 16*, Revision B.01; Gaussian, Inc., Wallingford CT, **2016**.
[34] Dovesi, R.; Erba, A.; Orlando, R.; Zicovich-Wilson, C. M.; Civalleri, B.; Maschio, L.; Rérat, M.; Casassa, S.; Baima, J.; Salustro, S.; Kirtman, B. Quantum-Mechanical Condensed Matter Simulations with CRYSTAL. *WIREs Comp. Mol. Sc.* **2018**, *8* (4), e1360.
[35] Dykstra, C. E.; Jasien, P. G. Derivative Hartree—Fock Theory to All Orders. *Chem. Phys. Lett.* **1984**, *109* (4), 388–393.
[36] Hurst, G. J. B.; Dupuis, M.; Clementi, E. Abinitio Analytic Polarizability, First and Second Hyperpolarizabilities of Large Conjugated Organic Molecules: Applications to Polyenes C4H6 to C22H24. *J. Chem. Phys.* **1988**, *89* (1), 385–395.
[37] Karamanis, P. The Importance of the DFT Method on the Computation of the Second Hyperpolarizability of Semiconductor Clusters of Increasing Size: A Critical Analysis on Prolate Aluminum Phosphide Clusters. *Int. J. Quant. Chem.* **2012**, *112* (9), 2115–2125.
[38] Karamanis, P.; Pouchan, C.; Weatherford, C. A.; Gutsev, G. L. Evolution of Properties in Prolate (GaAs)n Clusters. *J. Phys. Chem. C* **2011**, *115* (1), 97–107.
[39] Yanai, T.; Tew, D. P.; Handy, N. C. A New Hybrid Exchange–Correlation Functional Using the Coulomb-Attenuating Method (CAM-B3LYP). *Chem. Phys. Lett.* **2004**, *393* (1–3), 51–57.
[40] Henderson, T. M.; Izmaylov, A. F.; Scalmani, G.; Scuseria, G. E. Can Short-Range Hybrids Describe Long-Range-Dependent Properties? *J. Chem. Phys.* **2009**, *131* (4), 044108.
[41] Koch, H.; Jo/rgensen, P. Coupled Cluster Response Functions. *J. Chem. Phys.***1990**, *93* (5), 3333–3344.
[42] Grimme, S. Semiempirical Hybrid Density Functional with Perturbative Second-Order Correlation. *J. Chem. Phys.* **2006**, *124* (3), 034108.
[43] Brémond, É.; Sancho-García, J. C.; Pérez-Jiménez, Á. J.; Adamo, C. Communication: Double-Hybrid Functionals from Adiabatic-Connection: The QIDH Model. *J. Chem. Phys.***2014**, *141* (3), 031101.
[44] Lu, T.; Chen, F. Multiwfn: A Multifunctional Wavefunction Analyzer. *J. Comp. Chem. 33* (5), 580–592.

[45] Martin, R. L. Natural Transition Orbitals. *J. Chem. Phys.***2003**, *118* (11), 4775–4777.
[46] Karamanis, P.; Pouchan, C. Fullerene–C60 in Contact with Alkali Metal Clusters: Prototype Nano-Objects of Enhanced First Hyperpolarizabilities. *J. Phys. Chem. C* **2012**, *116* (21), 11808–11819.
[47] Otero, N.; Karamanis, P.; Pouchan, C. Hirshfeld-Based Atomic Population Analysis of the B, N Doping Effect in Zigzag Graphene Nanoribbons: $$\pi$$ Electron Density as Requirement to Follow the B, N Doping Guidelines. *Theor. Chem. Acc.* **2018**, *137* (2), 16..
[48] Otero, N.; Van Alsenoy, C.; Pouchan, C.; Karamanis, P. Hirshfeld-Based Intrinsic Polarizability Density Representations as a Tool to Analyze Molecular Polarizability. *J. Comput. Chem.* **2015**, *36* (24), 1831–1843.
[49] Karamanis, P.; Otero, N.; Pouchan, C. Electric Property Variations in Nanosized Hexagonal Boron Nitride/Graphene Hybrids. *J. Phys. Chem. C* **2015**, *119* (21), 11872–11885.
[50] Giambiagi, M.; Giambiagi, M. S. de; Silva, C. D. dos S.; Figueiredo, A. P. de. Multicenter Bond Indices as a Measure of Aromaticity. *Phys. Chem. Chem. Phys.* **2000**, *2* (15), 3381–3392.
[51] Bultinck, P.; Ponec, R.; Van Damme, S. Multicenter Bond Indices as a New Measure of Aromaticity in Polycyclic Aromatic Hydrocarbons. *J. Phys. Org. Chem.* **2005**, *18* (8), 706–718.
[52] Mandado, M.; González-Moa, M. J.; Mosquera, R. A. Chemical Graph Theory and N-Center Electron Delocalization Indices: A Study on Polycyclic Aromatic Hydrocarbons. *J. Comput. Chem.* **2007**, *28* (10), 1625–1633.
[53] Mandado, M.; González-Moa, M. J.; Mosquera, R. A. QTAIM N-Center Delocalization Indices as Descriptors of Aromaticity in Mono and Poly Heterocycles. *J. Comput. Chem.* **2007**, *28* (1), 127–136.
[54] Otero, N.; El-kelany, K. E.; Pouchan, C.; Rérat, M.; Karamanis, P. Establishing the Pivotal Role of Local Aromaticity in the Electronic Properties of Boron-Nitride Graphene Lateral Hybrids. *Phys. Chem. Chem. Phys.* **2016**, *18* (36), 25315–25328.
[55] Chattaraj, P. K.; Sengupta, S. Popular Electronic Structure Principles in a Dynamical Context. *J. Phys. Chem.* **1996**, *100* (40), 16126–16130.
[56] Hohm, U. Is There a Minimum Polarizability Principle in Chemical Reactions? *J. Phys. Chem. A* **2000**, *104* (36), 8418–8423.
[57] Rérat, M.; Maschio, L.; Kirtman, B.; Civalleri, B.; Dovesi, R. Computation of Second Harmonic Generation for Crystalline Urea and KDP. An Ab Initio Approach through the Coupled Perturbed Hartree–Fock/Kohn–Sham Scheme. *J. Chem. Theory Comput.* **2016**, *12* (1), 107–113.
[58] Champagne, B.; Perpète", É. A.; André, J.-M.; Kirtman, B. Analysis of the Vibrational Static and Dynamic Second Hyperpolarizabilities of Polyacetylene Chains. *Synthetic Metals* **1997**, *85* (1–3), 1047–1050. https://doi.org/10.1016/S0379-6779(97)80146-4.
[59] Bredas, J. L.; Adant, C.; Tackx, P.; Persoons, A.; Pierce, B. M. Third-Order Nonlinear Optical Response in Organic Materials: Theoretical and Experimental Aspects. *Chem. Rev.* **1994**, *94* (1), 243–278.
[60] Kuzyk, M. G.; Pérez-Moreno, J.; Shafei, S. Sum Rules and Scaling in Nonlinear Optics. *Physics Reports* **2013**, *529* (4), 297–398.
[61] Balaban, A. T.; Oniciu, D. C.; Katritzky, A. R. Aromaticity as a Cornerstone of Heterocyclic Chemistry. *Chem. Rev.* **2004**, *104* (5), 2777–2812.
[62] Seyler, H.; Purushothaman, B.; Jones, D. J.; Holmes, A. B.; Wong, W. W. H. Hexa-Peri-Hexabenzocoronene in Organic Electronics. *Pure Appl. Chem.* **2012**, *84* (4), 1047–1067.
[63] Wu, J.; Pisula, W.; Müllen, K. Graphenes as Potential Material for Electronics. *Chem. Rev.* **2007**, *107* (3), 718–747.
[64] Dumslaff, T.; Yang, B.; Maghsoumi, A.; Velpula, G.; Mali, K. S.; Castiglioni, C.; De Feyter, S.; Tommasini, M.; Narita, A.; Feng, X.; Müllen, K. Adding Four Extra K-Regions to Hexa-Peri-Hexabenzocoronene. *J. Am. Chem. Soc.* **2016**, *138* (14), 4726–4729.
[65] Otero, N.; Pouchan, C.; Karamanis, P. Quadratic Nonlinear Optical (NLO) Properties of Borazino (B3N3)-Doped Nanographenes. *J. Mater. Chem. C* **2017**, *5* (32), 8273–8287.
[66] Hirata, S.; Head-Gordon, M.; Szczepanski, J.; Vala, M. Time-Dependent Density Functional Study of the Electronic Excited States of Polycyclic Aromatic Hydrocarbon Radical Ions. *J. Phys. Chem. A* **2003**, *107* (24), 4940–4951.
[67] Miletić, T.; Fermi, A.; Orfanos, I.; Avramopoulos, A.; De Leo, F.; Demitri, N.; Bergamini, G.; Ceroni, P.; Papadopoulos, M. G.; Couris, S.; Bonifazi, D. Tailoring Colors by O Annulation of Polycyclic Aromatic Hydrocarbons. *Chem. Eur. J.* **2017**, *23* (10), 2363–2378.

[68] Naccarato, F.; Ricci, F.; Suntivich, J.; Hautier, G.; Wirtz, L.; Rignanese, G.-M. Searching for Materials with High Refractive Index and Wide Band Gap: A First-Principles High-Throughput Study. *Phys. Rev. Mat.* **2019**, *3* (4).

Table I. Dipole moment (μ_z) mean dipole polarizability ($\bar{\alpha}$) longitudinal first and second hyperpolarizabilities (β_{zzz}, γ_{zzzz}) and mean second hyperpolarizability (symbol) of PAB computed at various levels of theory using [MP2$^{(FULL)}$]/6-311++G(2d,2p) optimized nuclear geometries.

	μ_z	$\bar{\alpha}\times10^3$	$\beta_{zzzz}\times10^3$	$\gamma_{zzzz}\times10^6$	$\bar{\gamma}\times10^4$
6-311+G(2d,2p)					
HF	-3.61	144.8	2.6	0.45	11.2
MP2	-3.21	157.5	6.8	1.13	24.9
MP4	-3.18	157.1	7.1	1.24	26.7
CCSD	-3.31	150.4	5.0	0.81	18.1
CCSD(T)	-3.18	155.2	6.9	1.17	25.2
CAM-B3LYP	-3.23	157.8	6.7	0.80	17.8
LC-ωHPBE	-3.40	146.9	4.2	0.62	13.8

Table II. Hyperpolarizability comparisons between PAB and Ph_2 at several levels of theory with the 6-311+G(2d,2p) basis set.

	$\overline{\alpha}$		$(\gamma_{xxxx}, \gamma_{yyyy}) \times 10^4$		$\gamma_{zzzz} \times 10^6$		$\frac{\gamma_{zzzz}^{PyB}}{\gamma_{zzzz}^{Ph_2}}$	$\bar{\gamma} \times 10^4$		$\frac{\bar{\gamma}^{PAB}}{\bar{\gamma}^{Ph_2}}$
Method	Ph_2	PAB	Ph_2	PAB	Ph_2	PAB		Ph_2	PAB	
HF	137.5	144.8	2.2, 1.9	3.8, 2.1	0.08	0.45	5.6	3.3	11.2	3.4
MP2	140.5	157.5	2.4, 2.4	4.0, 2.6	0.11	1.14	10.4	4.7	24.9	5.3
CCSD	136.4	150.4	1.8, 2.2	3.5, 2.3	0.10	0.81	8.1	3.9	18.1	4.6
CCSD(T)	137.5	155.2	1.9, 2.4	3.8, 2.0	0.11	1.17	10.6	4.4	25.2	5.7
CAM-B3LYP	140.4	157.8	2.1, 2.2	3.3, 2.1	0.11	0.80	7.3	4.1	17.8	4.3
LC-ωHPBE	138.3	151.8	1.9, 1.9	2.8, 1.9	0.09	0.71	7.9	3.5	15.8	4.5

Table III. HOMO-LUMO gaps (HLG), vertical excitation energies of the first symmetry allowed excited state (E_{01}), and mean dipole (hyper)polarizabilities of the systems of **Fig. 7.** All values have been computed at the CAM-B3LYP level of theory.

	HLG	$E_{\lambda max}$	$\overline{\alpha}\times10^{3}$	$\gamma_{xxxx;\ yyyy}\times10^{6}$	$\gamma_{zzzz}\times10^{4}$	$\overline{\gamma}\times10^{6}$
$C_{150}H$	4.05	2.89	2.4	9.7	1.1	5.2
$C_{138}(BN)_6H$	3.88	2.70	2.4	11.2	1.7	6.0
$C_{138}(N\rightarrow B)_6H$	2.94	1.94	2.8	67.2	1.1	35.8
$C_{150}Ph$	4.05	2.88	3.0	16.2	3.2	8.8
$C_{138}(BN)_6Ph$	3.88	2.69	3.1	17.7	4.2	9.6
$C_{138}(N\rightarrow B)_6Ph$	2.68	1.76	3.7	189.2	3.1	100.8

FIGURES

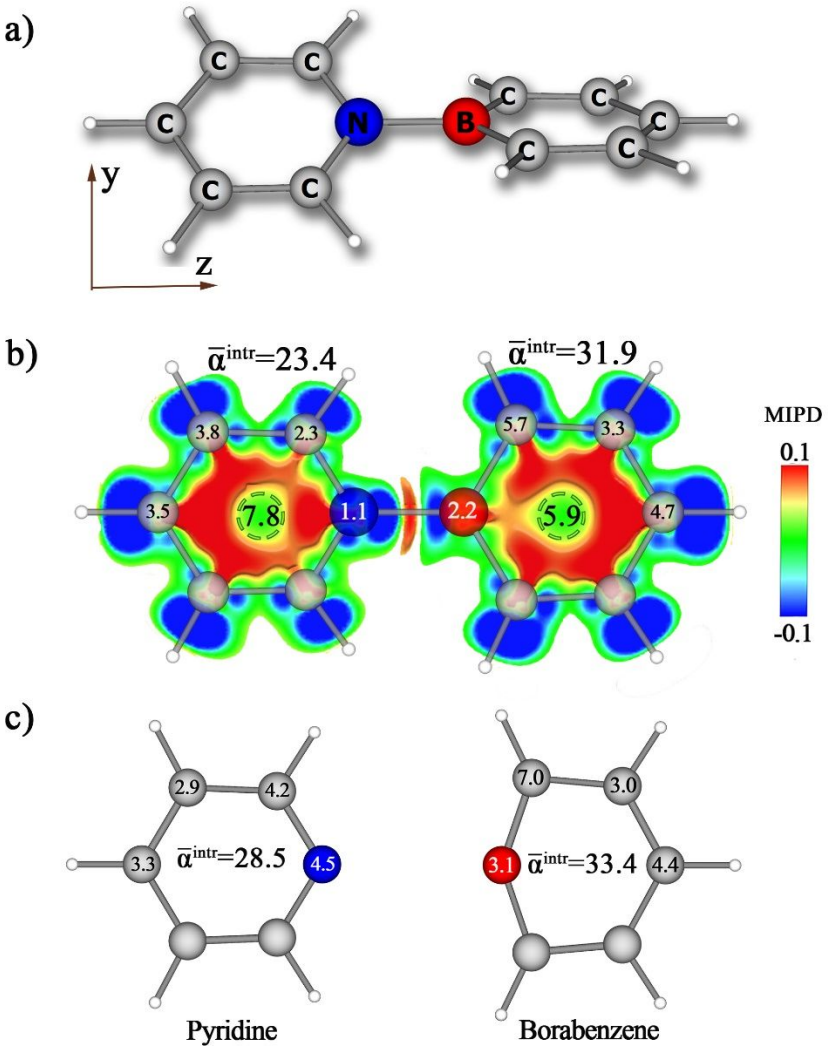

Figure 1. a) Molecular structure of PAB and the orientation used in this work. b) Mean intrinsic polarizabilities densities (MIPD) been projected on the plane each of the two ring-fragments and isotropic (mean) intrinsic atomic and fragment polarizabilities. Numbers in dashed cycles are the renormalized (*six*-center π-delocalization indices (*6*-Dis) representing the electron delocalization in rings. c) Atomic intrinsic polarizabilities of theisolated fragments. All properties have been obtained at CAM-B3LYP/6-311+G(2d,2p) level on MP2/6-311+G(2d,2p) optimized nuclear geometry taking into account all electrons of the molecules.

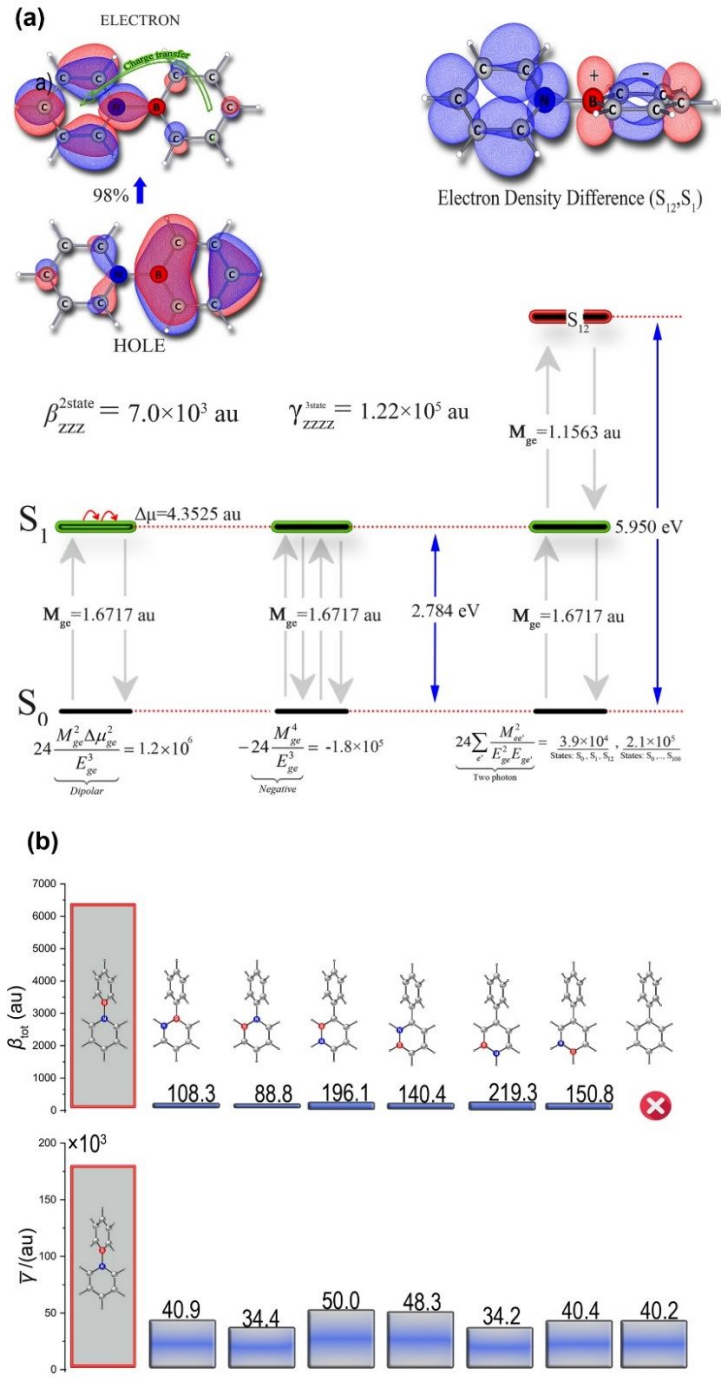

Fig. 2. (a) Dominant optical paths and charge transfer interaction dominating the first and second hyperpolarizability of PAB identified within the first 100 states of PAB at the LC-ωHPBE$^{\omega=0.3}$/6-311+G(2d,2p) level of theory. (b) First and second dipole hyperpolarizabilities of all possible isosteres of BN doped Ph2. All properties and equilibrium nuclear geometries have been obtained at the LC-ωHPBE$^{\omega=0.3}$/ 6-311+G(2d,2p) level of theory.

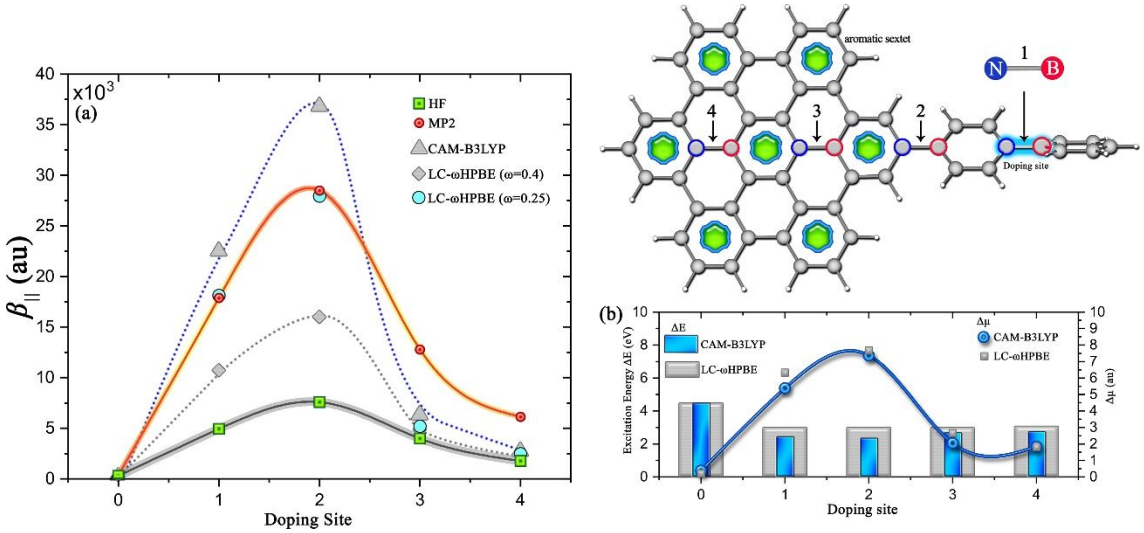

Fig. 3. (a) Evolution of the longitudinal component of the first dipole hyperpolarizability with respect to the doping site in hexa-benzo coronene (HBC) functionalized with one biphenyl unit. The nuclear geometries of each doped monomer have been relaxed at the CAM-B3LYP/6-31G(d) level including the Grimme's dispersion correction GD3 coefficient. The final equilibrium nuclear geometries of the pristine and doped Ph_2HBC are true local minima of quasi-planar shape characterized by real harmonic vibrational frequencies. (b) Evolution of the dipole moment difference between the ground and the first excited state of each Ph_2HBC BN isostere computed at the TD-CAM-B3LYP, -LC-ωHPBE (ω=0.30) levels with the 6-311G(d) basis set.

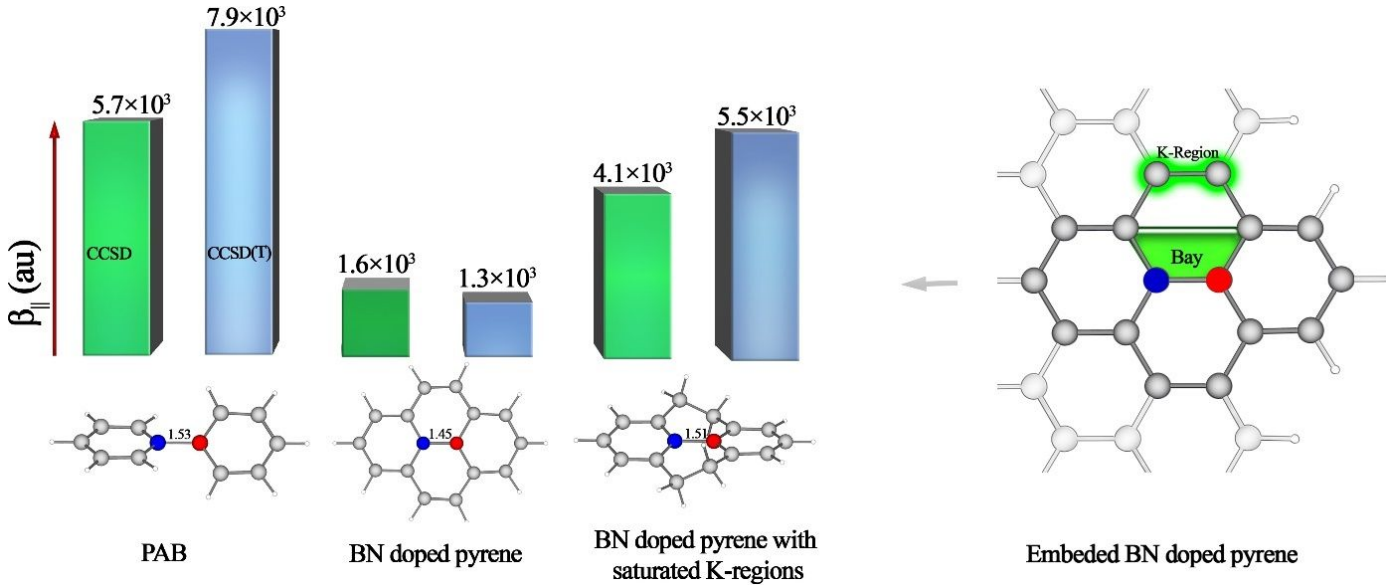

Fig. 4. Longitudinal first dipole hyperpolarizabilities of PAB, BN-doped-pyrene and its saturated derivative computed at the CCSD and CCSD(T) levels of theory with the 6-311+G(2d,2p) basis set. Hyperpolarizability values are given in atomic units and BN bond lengths in Å.

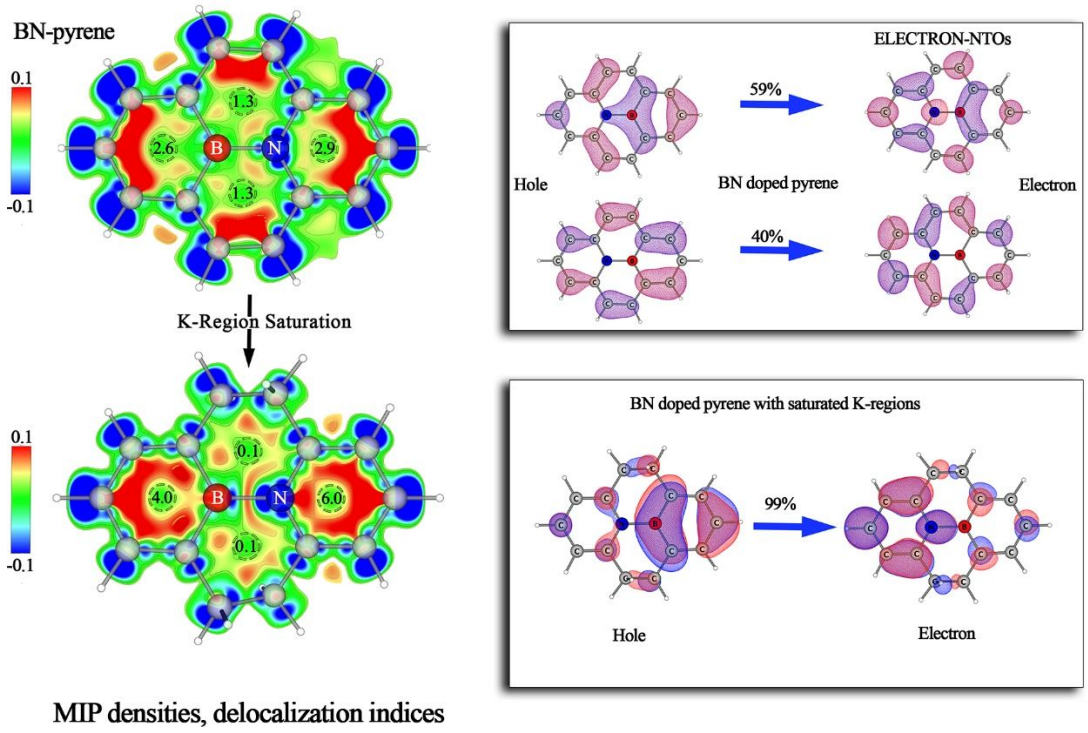

Fig. 5. Left, MIP densities and delocalization indices computed at the CAM-B3LYP/6-311+G(2d,2p) level of theory. Right, natural transition orbital pairs representing the dominant charge transfer excitations. Note that in (saturated) BNPYR the main transition can be described by (one) two NTOs accounting for the (99%) 99% of the total excitation.

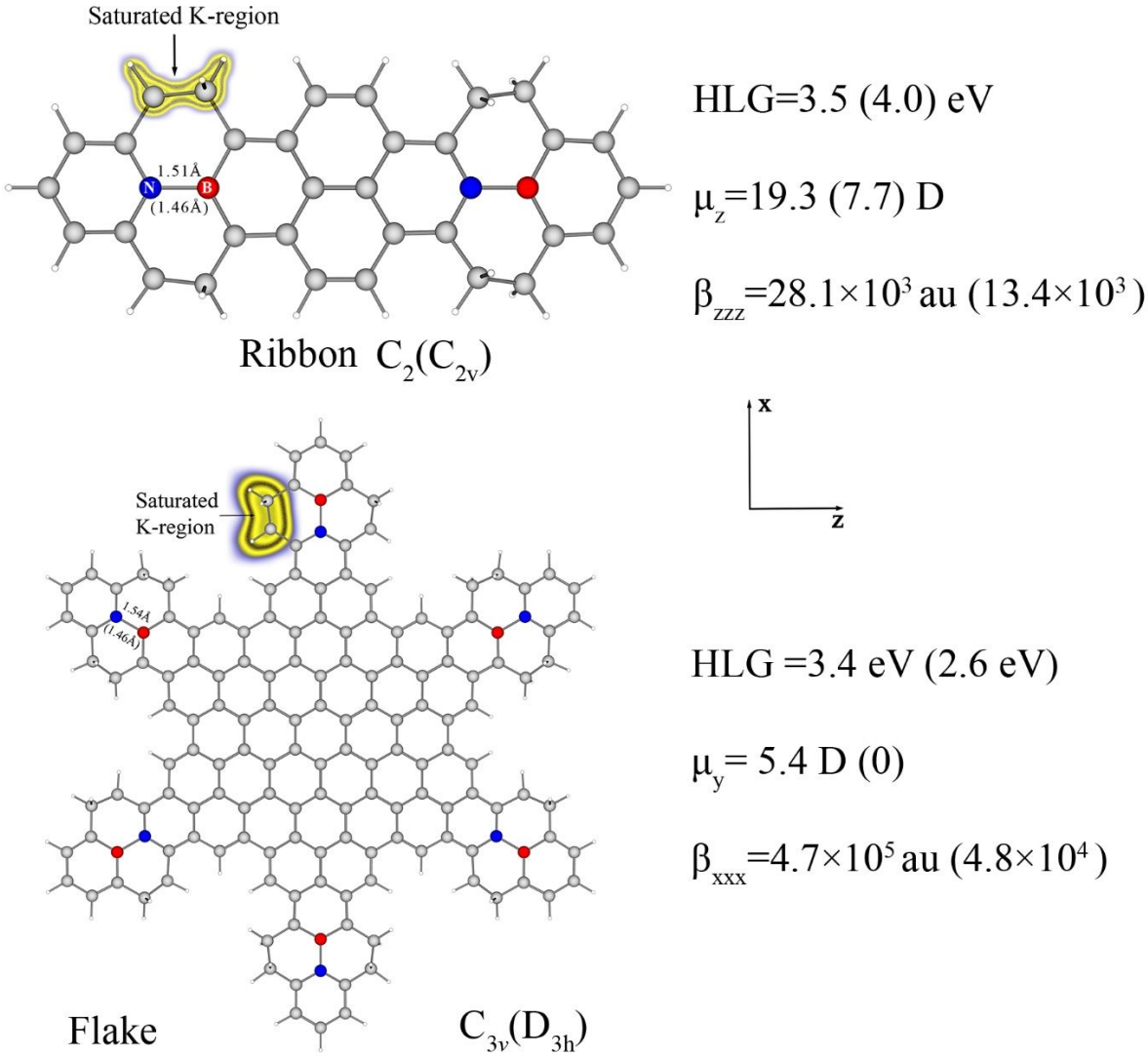

Fig. 6 Effect of the hydrogen saturation on the HOMO-LUMO gaps (HLG), dipole moments and dominant components of the first hyperpolarizabilities of two nanographene models doped with BN units. All computations have been performed at the CAM-B3LYP/6-311G(d) level. Number in parenthesis correspond to the properties of the all-carbon parental systems. Bond lengths in parenthesis correspond to the non-saturated species.

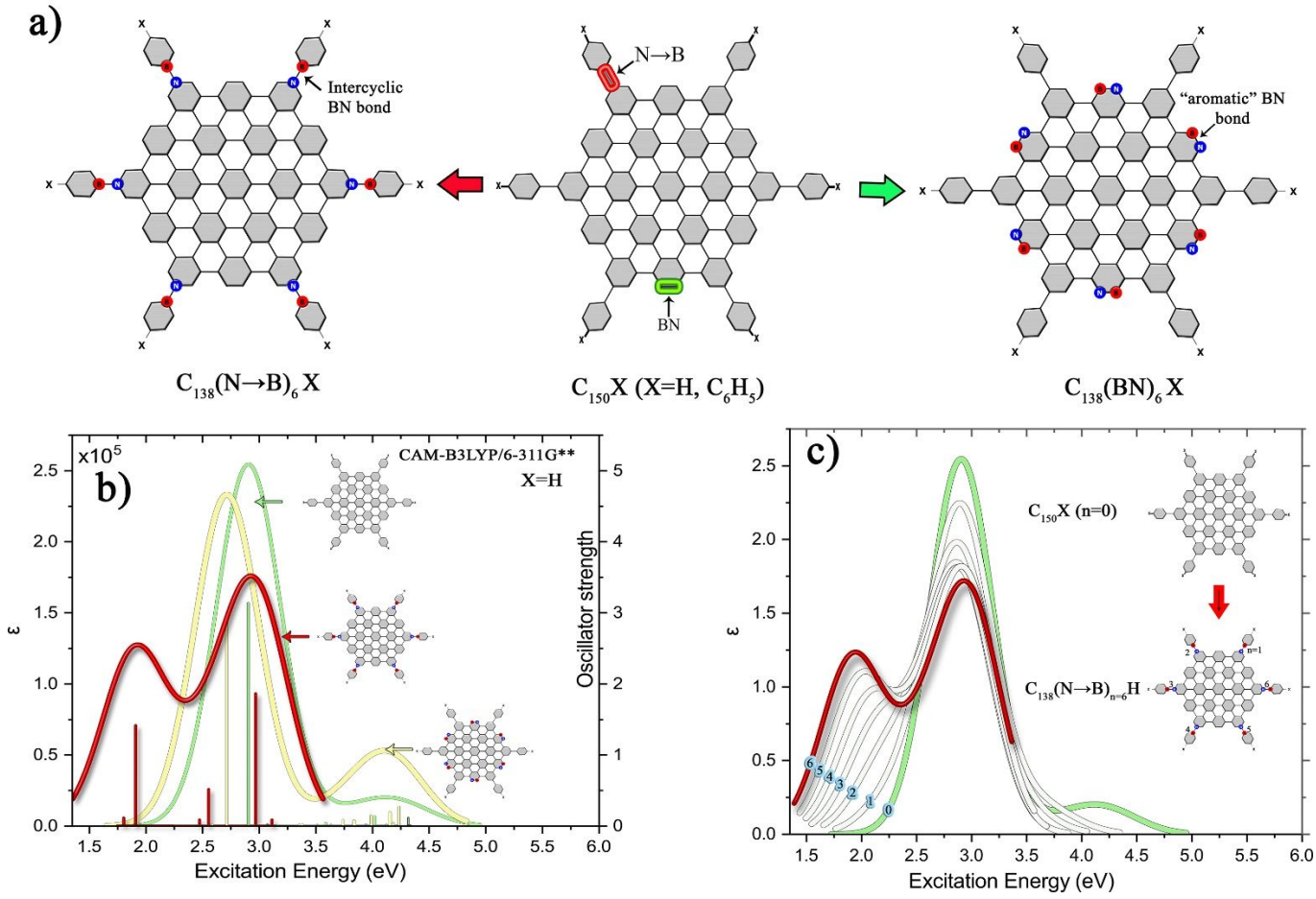

Fig. 7. a) BN and N→B doped nanographene models. b) and c) Simulated UV-VIS spectra within a spectral window between 0 to 6 eV of the systems BN and N→B doped nanographene models computed at the CAM-B3LYP/6-311G* level.

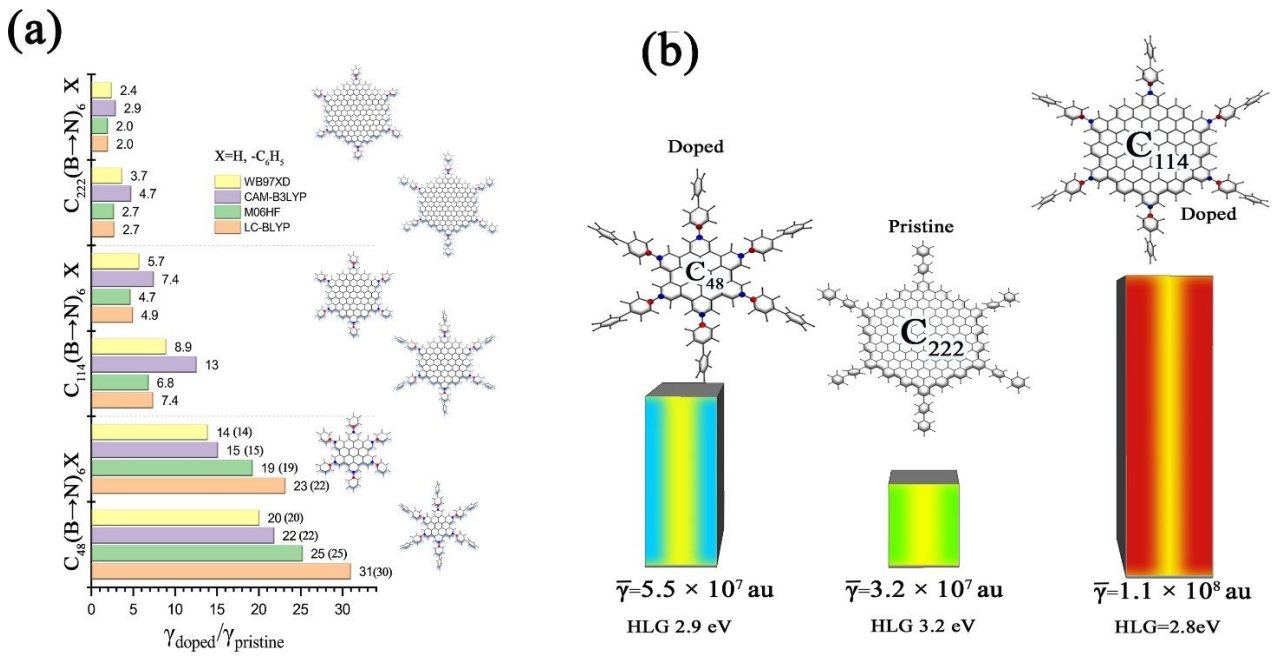

Fig. 8. a) Size dependence of the second dipole hyperpolarizability computed at various levels of theory and the 6-31G* basis set. Numbers in parenthesis correspond to values obtained with the 6-311+G(2d,2p) basis set. b) Hyperpolarizability comparisons between two doped and one pristine graphene flakes at the CAM-B3LYP 6-31G* level of theory.

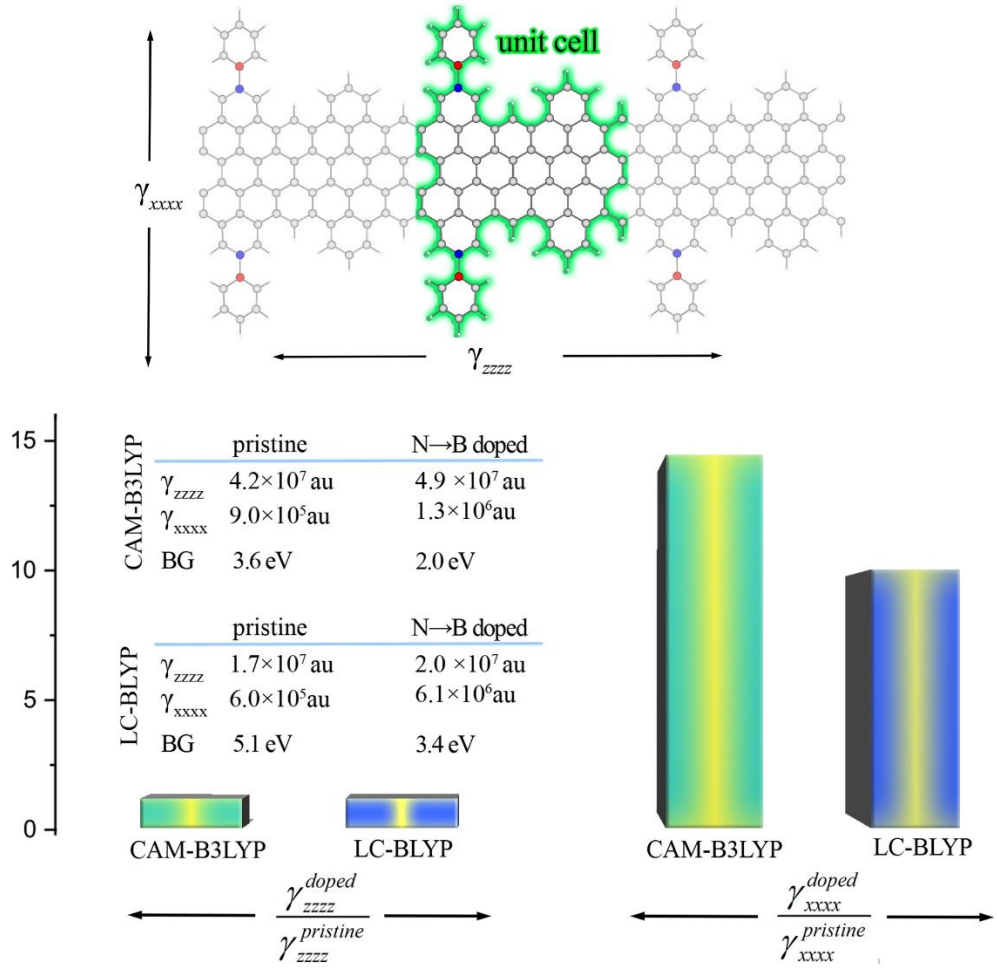

Fig. 9. Longitudinal second hyperpolarizabilities per unit cell of a graphene ribbon computed at the CAM-B3LYP and LC-BLYP levels of theory. The first Brillouin zone integration has been represented by the Monkhorst-Pack special k point method of 46 × 1 × 1 grid meshes for the cell. The energy convergence criteria for the self-consistent field was set to 10^{-7} Hartree. The basis set used here is pob_TZVP_2012 proposed by the developers of CRYSTAL 17.

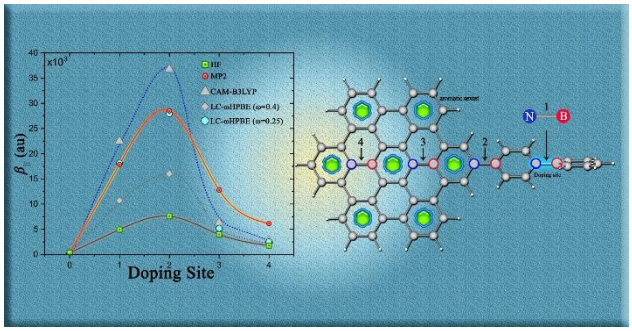
x10³
HF
MP2
CAM-B3LYP
LC-ωHPBE (ω=0.4)
LC-ωHPBE (ω=0.25)
β (au)
Doping Site
aromatic sextet
N
B

TOC Graphic

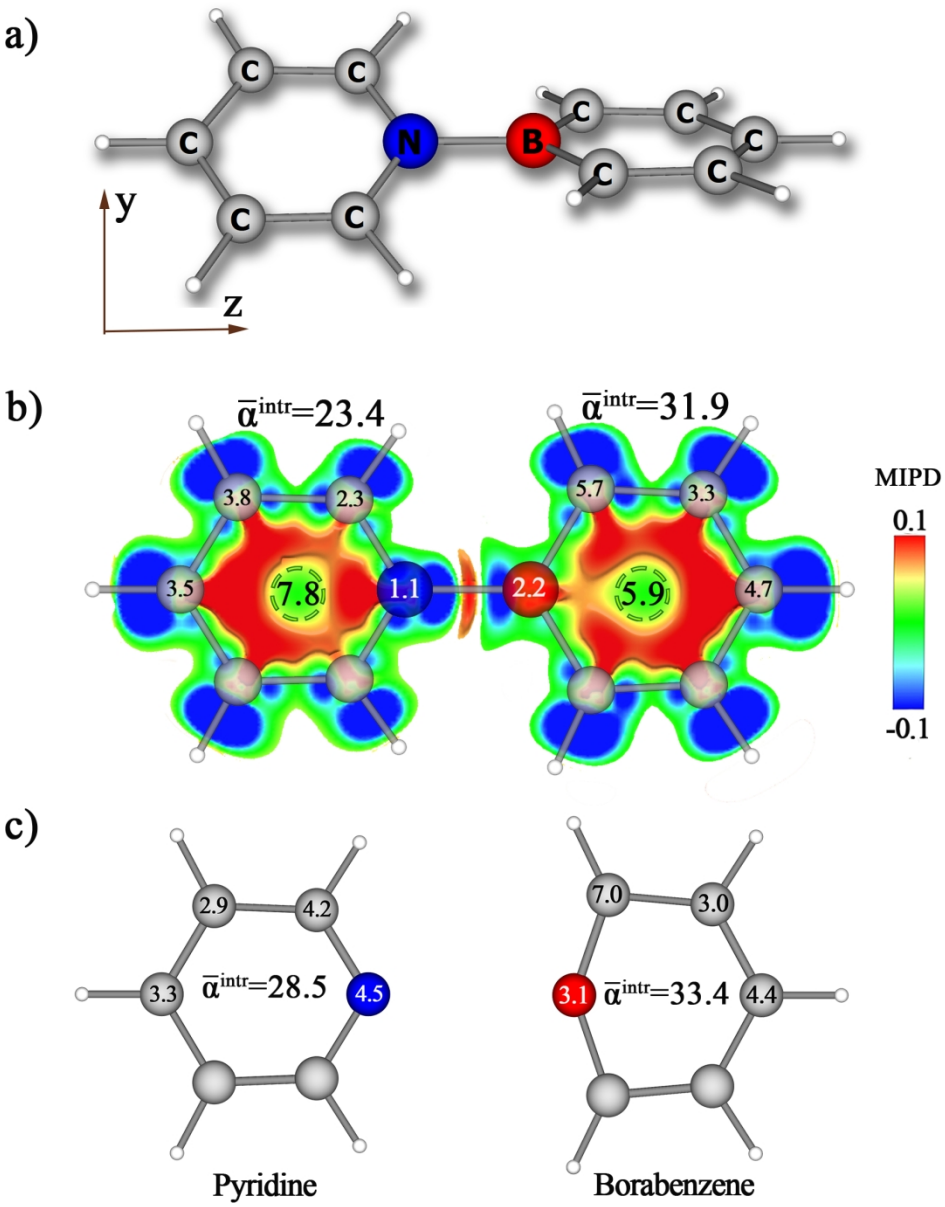

Figure 1. a) Molecular structure of PAB and the orientation used in this work. b) Mean intrinsic polarizabilities densities (MIPD) been projected on the plane each of the two ring-fragments and isotropic (mean) intrinsic atomic and fragment polarizabilities. Numbers in dashed cycles are the renormalized (the kind of renormalization employed should be indicated in the computational section, looking at the large numbers I do not figure out what has been applied) six-center π-delocalization indices (6-Dis) representing the electron delocalization in rings. c) I guess plot (c) represents the polarizabilities for the isolated fragments. All properties have been obtained at CAM-B3LYP/6-311+G(2d,2p) level on MP2/6-311+G(2d,2p) optimized nuclear geometry taking into account all electrons of the molecules.

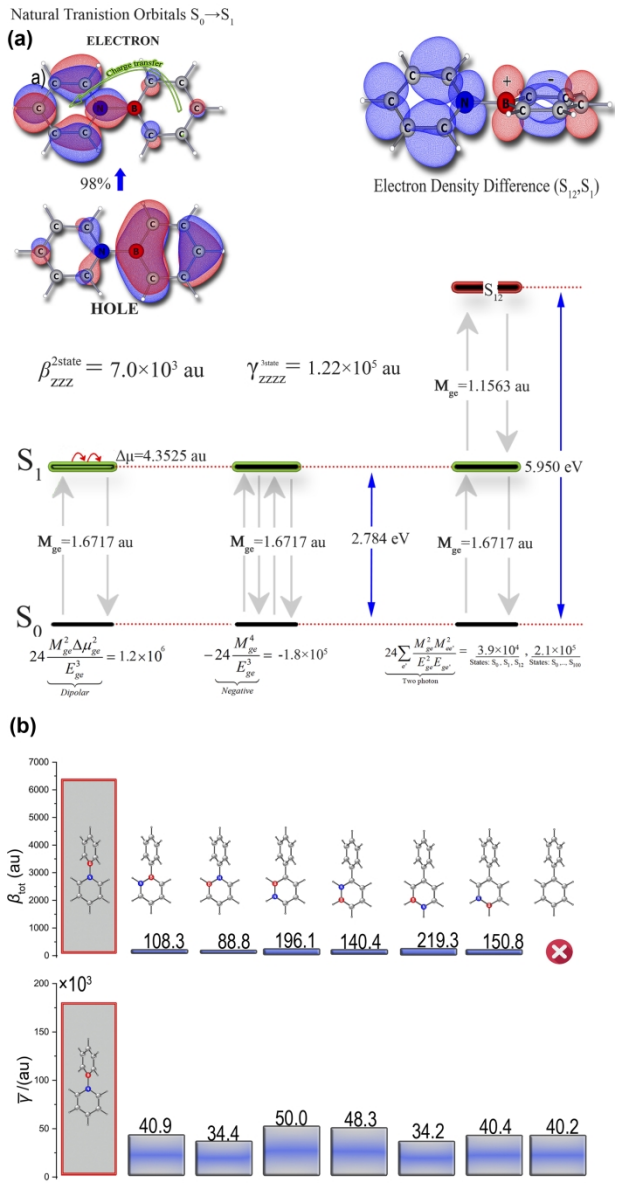

Fig. 2. (a) Dominant optical paths and charge transfer interaction dominating the first and second hyperpolarizability of PAB identified within the first 100 states of PAB at the LC-ωHPBEω=0.3/6-311+G(2d,2p) level of theory. (b) First and second dipole hyperpolarizabilities of all possible isosteres of BN doped Ph2. All properties and equilibrium nuclear geometries have been obtained at the LC-ωHPBEω=0.3/6-311+G(2d,2p) level of theory.

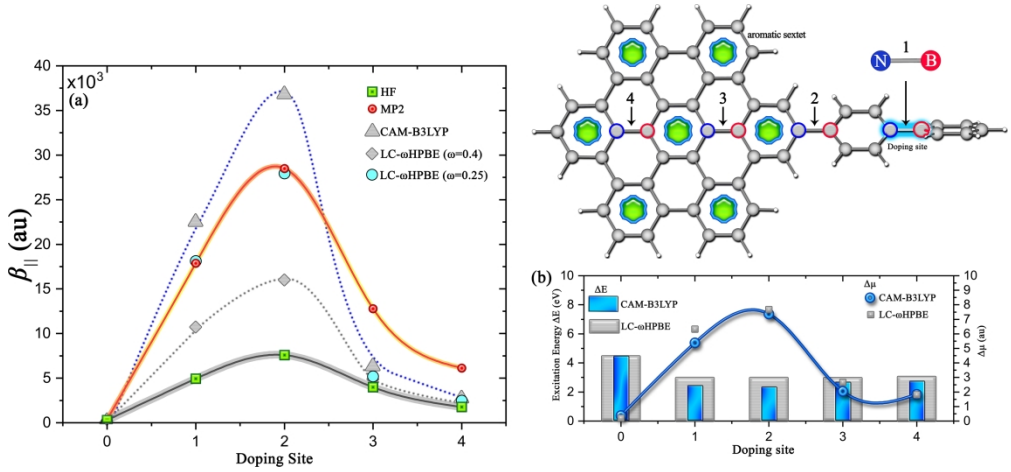

Table III. HOMO-LUMO gaps (HLG), vertical excitation energies of the first symmetry allowed excited state (E01), and mean dipole (hyper)polarizabilities of the systems of Fig. 7. All values have been computed at the CAM-B3LYP level of theory.

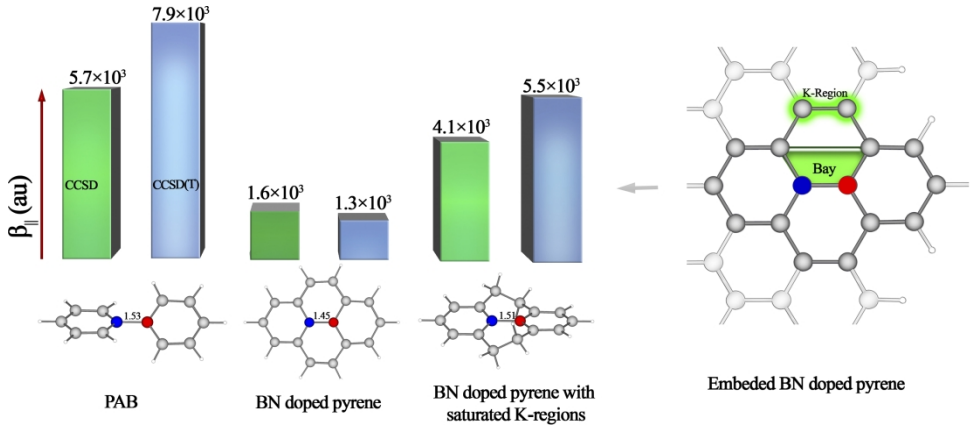

Fig. 4. Longitudinal first dipole hyperpolarizabilities of PAB, BN-doped-pyrene and its saturated derivative computed at the CCSD and CCSD(T) levels of theory with the 6-311+G(2d,2p) basis set. Hyperpolarizability values are given in atomic units and BN bond lengths in Å.

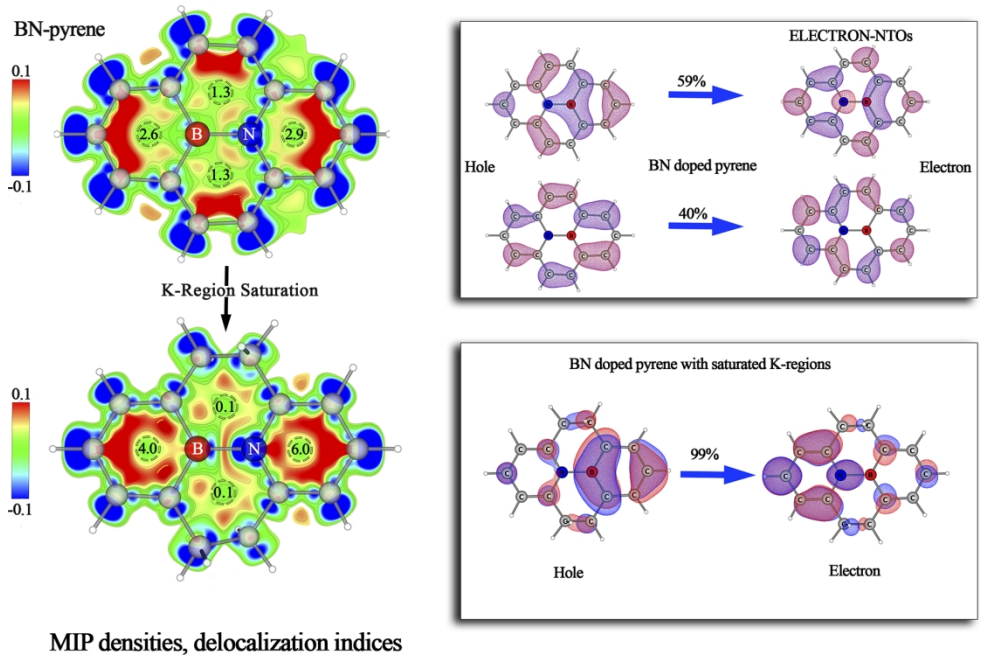

Fig. 5. Left, MIP densities and delocalization indices computed at the CAM-B3LYP/6-311+G(2d,2p) level of theory. Right, natural transition orbital pairs representing the dominant charge transfer excitations. Note that in (saturated) BNPYR the main transition can be described by (one) two NTOs accounting for the (99%) 99% of the total excitation.

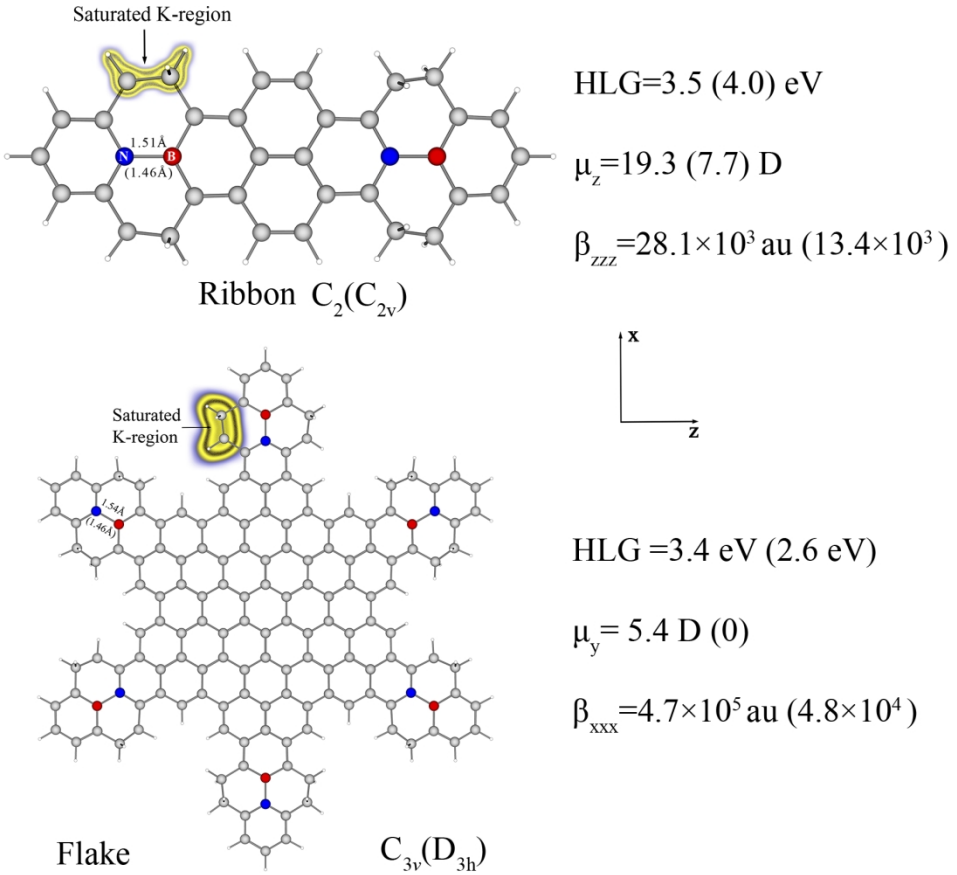

Fig. 6 Effect of the hydrogen saturation on the HOMO-LUMO gaps (HLG), dipole moments and dominant components of the first hyperpolarizabilities of two nanographene models doped with BN units. All computations have been performed at the CAM-B3LYP/6-311G(d) level. Number in parenthesis correspond to the properties of the all-carbon parental systems. Bond lengths in parenthesis correspond to the non-saturated species.

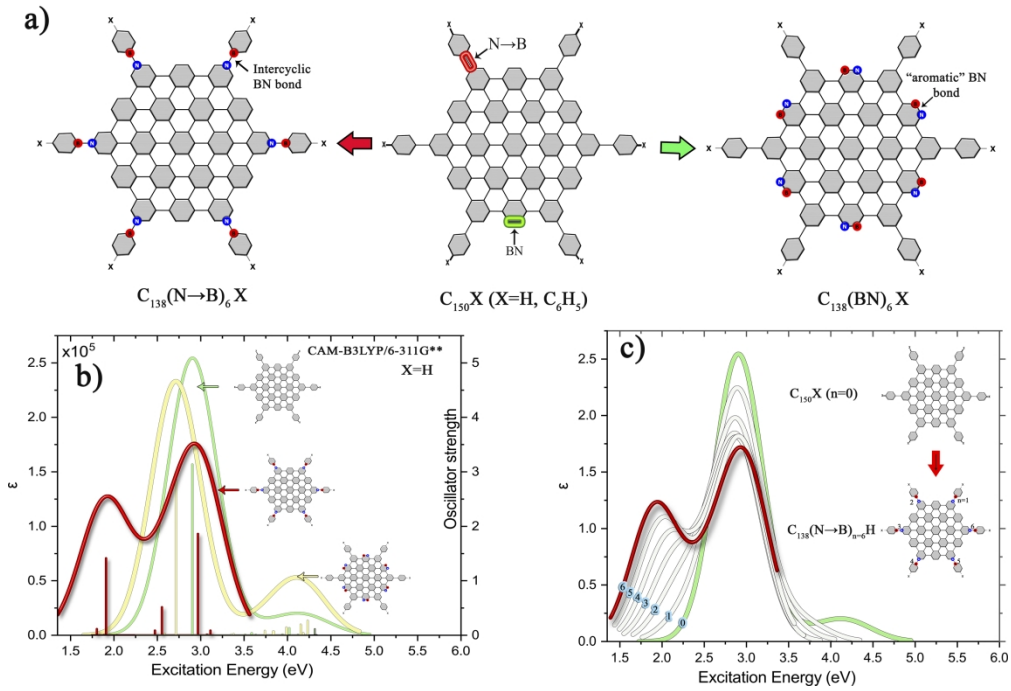

Fig. 7. a) BN and N→B doped nanographene models. b) and c) Simulated UV-VIS spectra within a spectral window between 0 to 6 eV of the systems BN and N→B doped nanographene models computed at the CAM-B3LYP/6-311G* level.

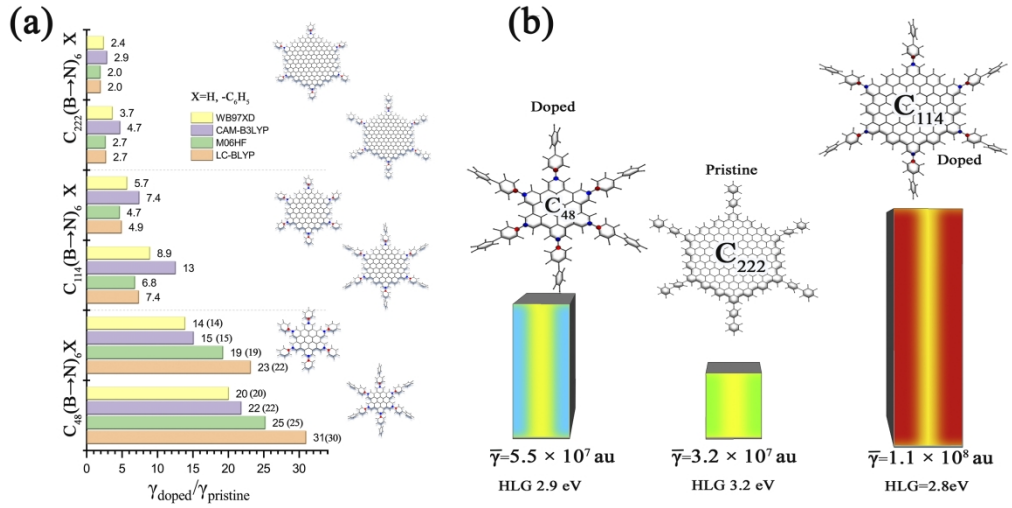

Fig. 8. a) Size dependence of the second dipole hyperpolarizability computed at various levels of theory and the 6-31G* basis set. Numbers in parenthesis correspond to values obtained with the 6-311+G(2d,2p) basis set. b) Hyperpolarizability comparisons between two doped and one pristine graphene flakes at the CAM-B3LYP 6-31G* level of theory.

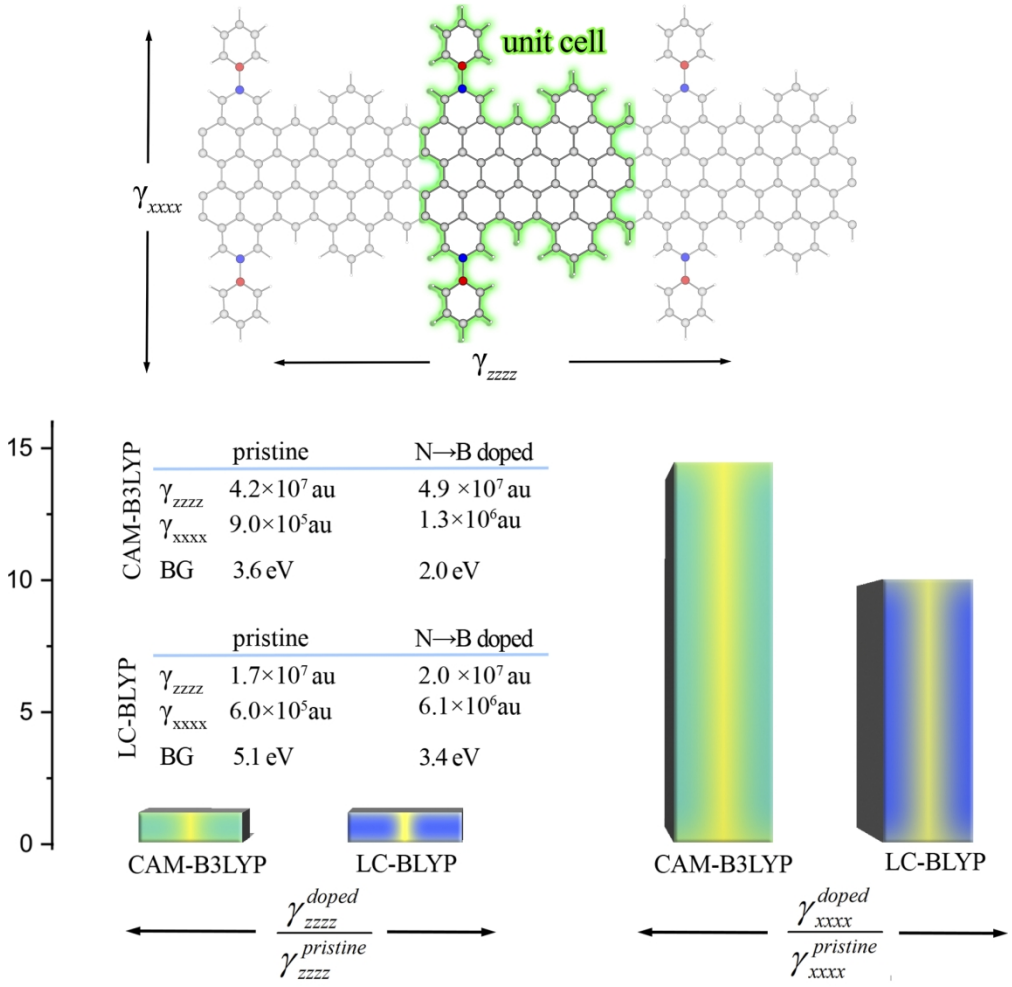

Fig. 9. Longitudinal second hyperpolarizabilities per unit cell of a graphene ribbon computed at the CAM-B3LYP and LC-BLYP levels of theory. The first Brillouin zone integration has been represented by the Monkhorst-Pack special k point method of 46 × 1 × 1 grid meshes for the cell. The energy convergence criteria for the self-consistent field was set to 10−7 Hartree. The basis set used here is pob_TZVP_2012 proposed by the developers of CRYSTAL 17.

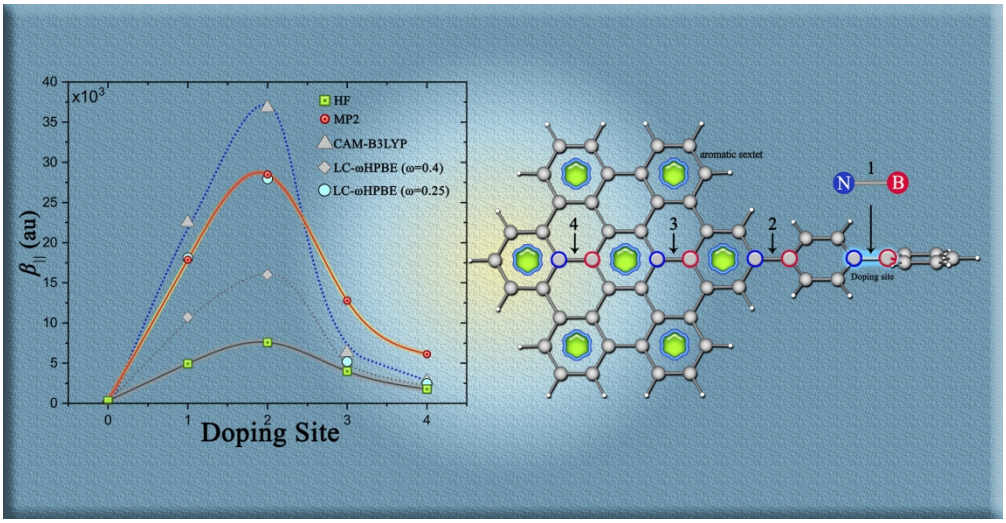
x10^3
HF
MP2
CAM-B3LYP
LC-ωHPBE (ω=0.4)
LC-ωHPBE (ω=0.25)
β|| (au)
Doping Site
aromatic sextet
N
B
1
2
3
4
Doping site